Effect of water vapor pressure on positive and negative tone electron-beam patterning of Poly (methyl methacrylate)

Running title: Effect of water vapor pressure on electron-beam patterning of PMMA

Running Authors: Kumar et al.

Deepak Kumar[1, a)], Krishnaroop Chaudhuri[3], Joseph W. Brill[2], Jonathan T. Pham[3], J. Todd Hastings[1,2 b)]

[1] Department of Electrical and Computer Engineering, University of Kentucky, Lexington, KY 40506, United States of America
[2] Department of Physics and Astronomy, University of Kentucky, Lexington, KY 40506, United States of America
[3] Department of Chemical and Materials Engineering, University of Kentucky, Lexington, KY 40506, United States of America

a) Electronic mail: deepak.kumar@uky.edu

b) Electronic mail: todd.hastings@uky.edu

Variable-pressure electron-beam lithography (VP-EBL) employs an ambient gas at sub–atmospheric pressures to reduce charging during electron-beam lithography. VP-EBL has been previously shown to eliminate pattern distortion and provide improved resolution when patterning PMMA on insulating substrates. However, it remains unknown how water vapor affects the contrast and clearing dose, nor has the effect of water vapor on the negative–tone behavior of PMMA been studied. In addition, water vapor was recently shown to alter the radiation chemistry of the VP-EBL process for Teflon AF. Such changes in radiation chemistry have not been explored for PMMA. In this work, VP-EBL was conducted on conductive substrates to study the effect of water vapor on PMMA patterning separately from the effects of charge dissipation. In addition, both positive and negative tone processes were studied to determine the effect of water vapor on both chain scission and cross-linking. The contrast of PMMA was found to improve significantly with increasing water vapor pressure for both positive and negative tone patterning. The clearing

dose for positive tone patterning increases moderately with vapor pressure as would be expected for electron scattering in a gas. However, the onset set dose for negative tone patterning increased dramatically with pressure revealing a more significant change in the exposure mechanism. X-ray photoelectron spectra and infrared transmission spectra indicate that water vapor only slightly alters the composition of exposed PMMA. Also, electron scattering in water vapor yielded a much larger clear region around negative-tone patterns. This effect could be useful for increasing the range of the developed region around cross-linked PMMA beyond the backscattered electron range. Thus, VP-EBL for PMMA introduces a new means of tuning clearing/onset dose and contrast, while allowing additional control over the size of the cleared region around negative-tone patterns.

I. INTRODUCTION

Electron beam irradiation is a versatile method of modifying materials and forms the bases for electron-beam lithography of both organic and inorganic resists.[1–18] Poly (methyl methacrylate), PMMA, is the most widely used electron-beam resist due to its high resolution and stability.[19] It is well known that upon electron beam irradiation at lower exposure doses, PMMA acts as a positive resist due to chain scission of the polymer. At higher exposure doses both cross-linking and compositional changes in PMMA produce to negative-tone resist behavior.[20–24]

Variable-pressure electron-beam lithography (VP-EBL) employs an ambient gas at sub–atmospheric pressures to reduce charging during electron-beam lithography. Previous work demonstrated that VP-EBL can eliminate distortion and improve resolution when patterning PMMA on insulating substrates[25]. However, it remains unknown how water vapor pressure affects the contrast and clearing dose, nor has anyone studied the effects of water vapor pressure on the negative–tone behavior of PMMA. In addition, water vapor was recently shown to alter the

radiation chemistry of the VP-EBL process for Teflon AF, an amorphous fluorinated polymer that can function as a positive or negative resist.[26] Such changes in radiation chemistry have not been explored for VP-EBL of PMMA.

In this work, through systematically studying the effect of water vapor pressure on both the positive and negative tone behavior of PMMA, we show that water vapor alters both the sensitivity and contrast of PMMA for both positive- and negative- tone processes. We find that water vapor only slightly changes the composition of exposed PMMA, and thus hypothesize that changes in sensitivity and contrast are associated with changes in distributions of molecular weight. We also show that the skirting effect of forward scattering of electrons in the water vapor[27] can control the size of the cleared region around negative tone patterns providing an alternative to large area positive tone writing.

II. EXPERIMENTAL

A. Spin Coating

PMMA (950 K molecular weight, MicroChem Corp.) was diluted using Anisole (MicroChem Corp.) to make 4 wt.% solution. The PMMA solution thus prepared was spin-coated onto a n-type <100> silicon substrate at 500 rpm for 5 seconds to give a uniform layer and then spun at 4000 rpm for 1 minute to set the desired thickness. Next, the spin-coated Si substrate was heated on a hot plate at 180ºC for 120 seconds to remove any residual solvent. Ellipsometry (M-2000, J. A. Woollam Co. Inc.) was used to measure the film thickness of the spin-coated PMMA film.

B. Variable-Pressure Electron Beam Lithography process

An ELPHY Plus pattern generator (Raith GmbH) coupled with FEI environmental scanning electron microscope (Quantum FEG 250) with a fast beam blanker was used for VP-EBL process. The analytical working distance of 10 mm and beam energy of 30 keV was used for all lithographic processes. A faraday cup and a pico-ammeter (Keathley 6487) were used for the beam current measurements under high vacuum conditions prior to each lithographic exposure. Gold nanoparticles deposited onto PMMA were used for focusing and as marker during patterning.

For the positive tone process, 20 μm x 100 μm rectangular structures were exposed under high vacuum and water vapor (0.1 mbar, 1 mbar, 3 mbar and 10 mbar) with areal exposure dose ranging from 10 – 300 μC cm^{-2} with a step size of 12.8 nm and beam current of 93 pA. An electron beam energy of 30 keV was chosen to reduce beam scattering in both the water vapor and resist, as well as to distribute backscattering to the largest range possible.[28] Each adjacent rectangle was given a 20 μm spacing to minimize proximity effects from backscattering. The exposed film was developed in 1:3 MiBK: IPA for 60 seconds at 18˚C followed by 30 seconds IPA rinse. Thickness measurements of the resulting resist surface were conducted using a Dektak 6M (Veeco, Inc.) surface profiler.

For the negative tone process, first an array of single-pixel dots were exposed from 60 fC – 9 pC under high vacuum and water vapor (0.1 mbar, 1 mbar, 3 mbar and 10 mbar) to estimate the onset areal dose. Then an array of 20 rectangles (5 μm x 50 μm) was exposed under the same conditions with an areal exposure dose from 1 – 40 mC cm^{-2} with a 12.8 nm step size and a beam current of 414 pA. The film was developed in 1:2 MiBK: IPA for 60 seconds at 18˚C followed by 30 seconds IPA rinse. 1:2 MiBK: IPA is typically used in the negative tone process to provide a slightly larger cleared area.[21] Additional features, numbers with arrow signs exposed at 20 mC cm^{-2}, were included close to the desired pattern and were used as markers for atomic force microscopy

(AFM) measurements. For thickness measurements, AFM was performed using JPK Nanowizard 4 equipped with standard silicon cantilevers with pyramidal tips.

For the positive tone process, samples for Fourier-transform infrared (FTIR) spectroscopy were prepared by exposing 200 μm x 200 μm rectangular structures under high vacuum and water vapor (0.1 mbar, 1 mbar, 3 mbar and 10 mbar) with areal exposure doses of 100 μC cm^{-2} and 175 μC cm^{-2} using a step size of 12.8 nm and beam current of 110 pA. Two different doses were chosen to accommodate the clearing dose for all vapor pressures. For the negative tone process, samples were prepared for FTIR spectroscopy by exposing 250 μm x 250 μm rectangular structures under high vacuum and 1 mbar water vapor with areal exposure doses of 15 mC cm^{-2} and 40 mC cm^{-2} using a step size of 12.8 nm and beam current of 5.9 nA. The beam current and structure size varied between experiments to keep exposure times to a reasonable duration. The difference in beam current used for FTIR samples for the positive tone patterns arises from small changes in beam current over the course of the study. The experimental conditions are tabulated in Table 1.

Table 1 Experimental conditions

	Chamber pressure	Beam Current (nA)	Exposure Dose (mC cm^{-2})	Pattern size	Developer
Positive tone	Vacuum and 0.1 – 10 mbar water vapor	0.093	0.01 – 0.3	20 µm x 100 µm	1:3 MiBK: IPA
Negative tone	Vacuum and 0.1 – 10 mbar water vapor	0.414	1 – 40	5 µm x 50 µm	1:2 MiBK: IPA
FTIR Positive tone	Vacuum and 0.1 – 10 mbar water vapor	0.110	0.1 and 0.175	200 µm x 200 µm	No development
XPS and FTIR Negative tone	Vacuum and 1 mbar water vapor	5.9	15 and 40	250 µm x 250 µm	1:2 MiBK: IPA

C. *X-ray photoelectron spectroscopy*

A Thermo Scientific K-Alpha X-ray Photoelectron Spectrometer was used for surface analysis. X-ray photoelectron spectroscopy (XPS) was performed on as-coated PMMA samples and samples exposed at high doses under high vacuum and under 1mbar water vapor. An areal exposure dose of 40 mC cm^{-2} was used for patterning XPS samples. In both cases, we sputter the surface of the PMMA with argon ions to remove any adventitious carbon. Preliminary peak fitting was conducted in Thermo Advantage software. Final fitting was completed using custom Python code based on the lmfit module[29] which allowed detailed error analysis. Details of the peak fitting strategies for the various samples are provided in Section III.B.4.

D. Fourier-transform infrared spectroscopy

A Thermo Fisher Scientific Nicolet 6700 FTIR spectrometer coupled to an infrared microscope was used to acquire the infrared transmission spectra. For the positive tone process, measurements were taken for undeveloped samples. For negative tone FTIR spectroscopy, measurements were taken both before and after sample development. Larger patterns were exposed for samples prepared for FTIR measurements to meet the minimum spot size requirement of the instrument. During measurements, the illuminated region was well within the exposed region. Transmission spectra were acquired for as-coated PMMA and exposed patterns.

III. RESULTS AND DISCUSSIONS

PMMA films were spin coated onto silicon substrates and exposed at varying electron-beam currents, areal doses (charge/area), and water vapor pressures. This work was conducted to study the effect of water vapor pressure on both the positive and negative tone behavior of PMMA. Contrast curves were obtained to observe changes in the contrast and sensitivity under water vapor. SEM (Scanning Electron Microscopy), XPS analysis, and Fourier-transform infrared spectroscopy analysis were performed on the exposed patterns before and after development to measure changes in surface and chemical composition as a function of exposure conditions.

A. Effect of water vapor on e-beam patterning of PMMA in the positive tone process

The increased solubility of the exposed areas in a developer caused by the degradation of PMMA by electron beam makes it a suitable candidate as a positive e-beam resist. Main chain

scission in PMMA can result from cleavage of the methyl ester side-group to form a polymer radical, path (i) in Fig. 1, and has been found to be the major initiator of polymer degradation. The cleaved methyl ester side-group then either undergoes further decomposition leading to the release of CO, CO_2, CH_4, CH_3OH, etc. or combines with other radicals. This is followed by the competitive processes of main chain scission or hydrogen abstraction, paths (ii) and (iv). Hydrogen abstraction results in a double bond formation in the main chain or side group. Main chain scission can also result from direct action of a primary or secondary electron on a C-C bond shown by path (iii) but not been found to be the major initiator of polymer degradation.

1. Positive tone contrast curves

To study the effect of water vapor pressure on positive–tone behavior, the contrast values of the exposed and developed pattern were measured. The positive tone contrast curves, normalized residual resist thickness, NRT, vs. areal exposure dose, D, are plotted for different water vapor pressures in Fig. 2. No significant relief pattern before development was observed under either high vacuum or water vapor indicating that no direct etching of the PMMA is occurring in this dose range.

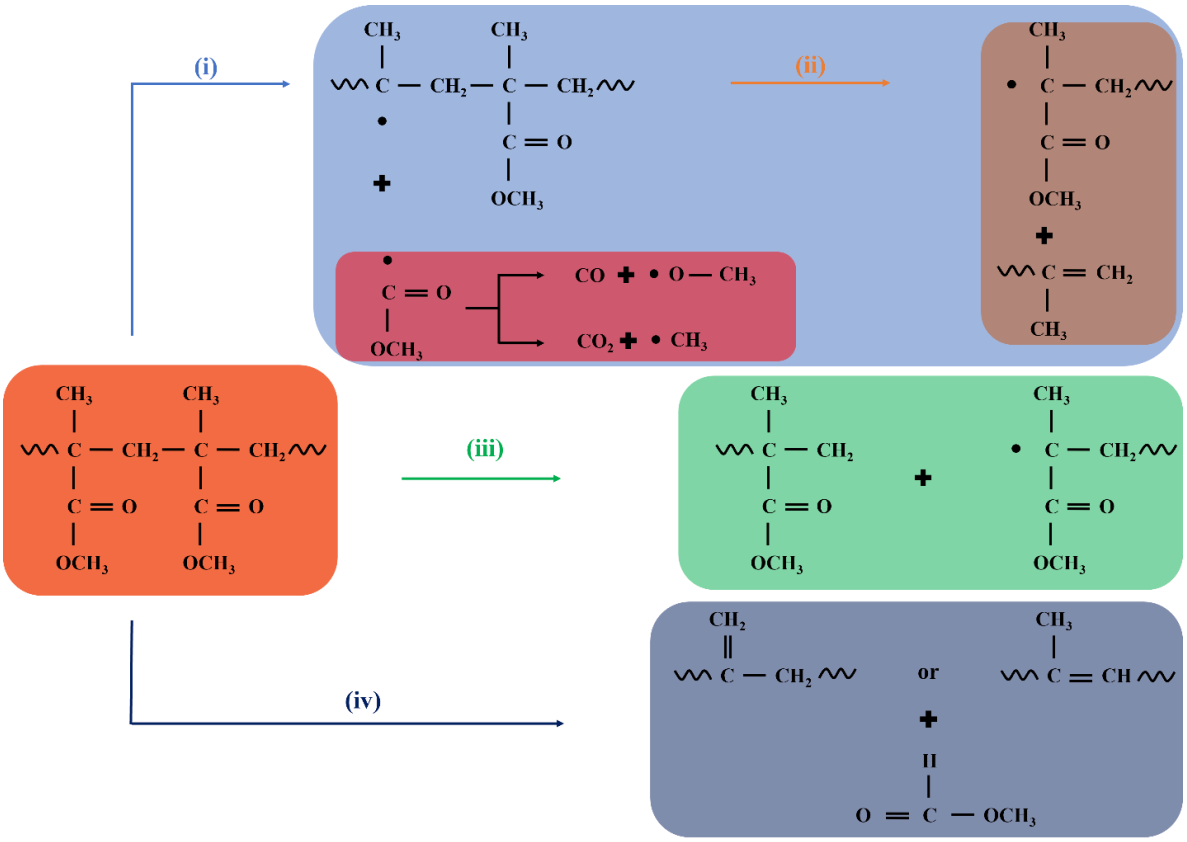

Figure 1. Schematics showing possible reaction paths for radiation damage in PMMA, as described in Ref 30–32. Cleavage of the methyl ester group (i) by a primary or secondary electron leads to subsequent main chain scission (ii) or C=C bond formation by hydrogen abstraction (iv). Direct action of an electron can also lead to main chain scission (iii).

The dose to clear, D_C, and contrast, γ, in Fig. 3 were obtained by fitting the data in to an empirical model of the form[33]

$$\mathrm{NRT} = C_0 - e^{S(D-D_C)} \qquad (1)$$

where C_0, S, and D_C are fitting parameters. For most cases, $C_0 \approx 1$. S is a factor that defines how sharply the curve changes as a function of dose; and D_c is the dose to clear. The contrast, γ, can be obtained from[33]

$$\gamma = \ln(10)\ S\ D_c \qquad (2)$$

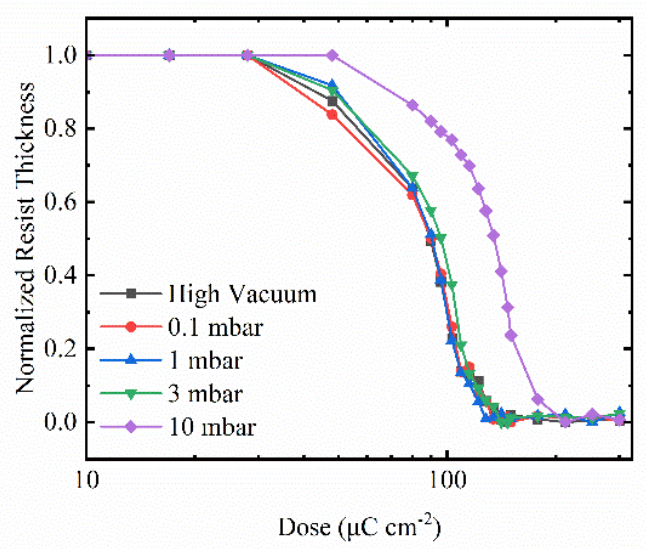

Figure 2. Normalized residual resist thickness vs. exposure dose (experimental values) for PMMA exposed under high vacuum and water vapor pressures ranging from 0.1 to 10 mbar.

The experimental data and fitted curves for each water vapor pressure are shown in Figure 3. Data points not well modeled by Eqn. (1), i.e., those with small or zero residual resist thickness, were excluded from the fitting process and are marked by an "×". Standard errors of the fitting parameters were calculated from the diagonal entries of the covariance matrix. Table 2 summarizes the contrast and dose to clear for exposure under high vacuum and each water vapor pressure. Figure 4 plots these parameters vs. water vapor pressure.

We note that the absolute values for contrast and clearing dose could be affected by proximity effects. The spacing of the features (20 μm) is sufficient that exposure by backscattered electrons will have a small effect at 30 keV. However, forward scattering in water vapor, especially at higher pressures, may have a more significant effect. Danilatos[34] showed that the beam skirt radius from plural scattering in a gas can be approximated by

$$R_s = 364 \left(\frac{Z}{E}\right)\left(\frac{P}{T}\right)^{1/2} L^{3/2} \qquad (3)$$

where a circle of radius R_S, in meters, encompasses 90% of the scattered electrons, Z is the effective atomic number (7.42 for water vapor[27]) of the scatterer, E is the primary electron energy in eV, P is the pressure in pascals, T is the temperature in Kelvin, and L is the gas path length in meters. For the conditions considered here, the skirt radius ranges from 16 μm at 0.1 mbar to 160 μm at 10 mbar. Clearly, proximity effects arising from gas scattering will alter the measured dose to clear for all but the high vacuum and 1 mbar data.

Upon introducing water vapor, the contrast decreases and then increases steadily with increasing water vapor pressure. An empirical line fit of the form $\gamma = \alpha + \beta \cdot \ln\left(\frac{P_{H_2O}}{1mbar}\right)$ with $\alpha = 6.9 \pm 0.06$ and $\beta = 0.50 \pm 0.03$ indicates that there is a statistically significant increase in contrast with water vapor pressure as shown in Figure 4(a). Thus, the transition of the exposed region from insoluble to soluble in a developer solution is found to be sharper with increasing water vapor pressure. This change in differential solubility of the exposed PMMA could arise from changes in chemical composition or from changes in the molecular weight distribution as discussed in Section III.A.2 below. The increase in dose to clear with water vapor pressure is shown in Figure 4(b). The dose to clear increases sharply beyond 3 mbar. This reduction in sensitivity could be simply the result of electron scattering in the water vapor[35] or could be related to changes in composition or molecular weight in the exposed PMMA as discussed below.

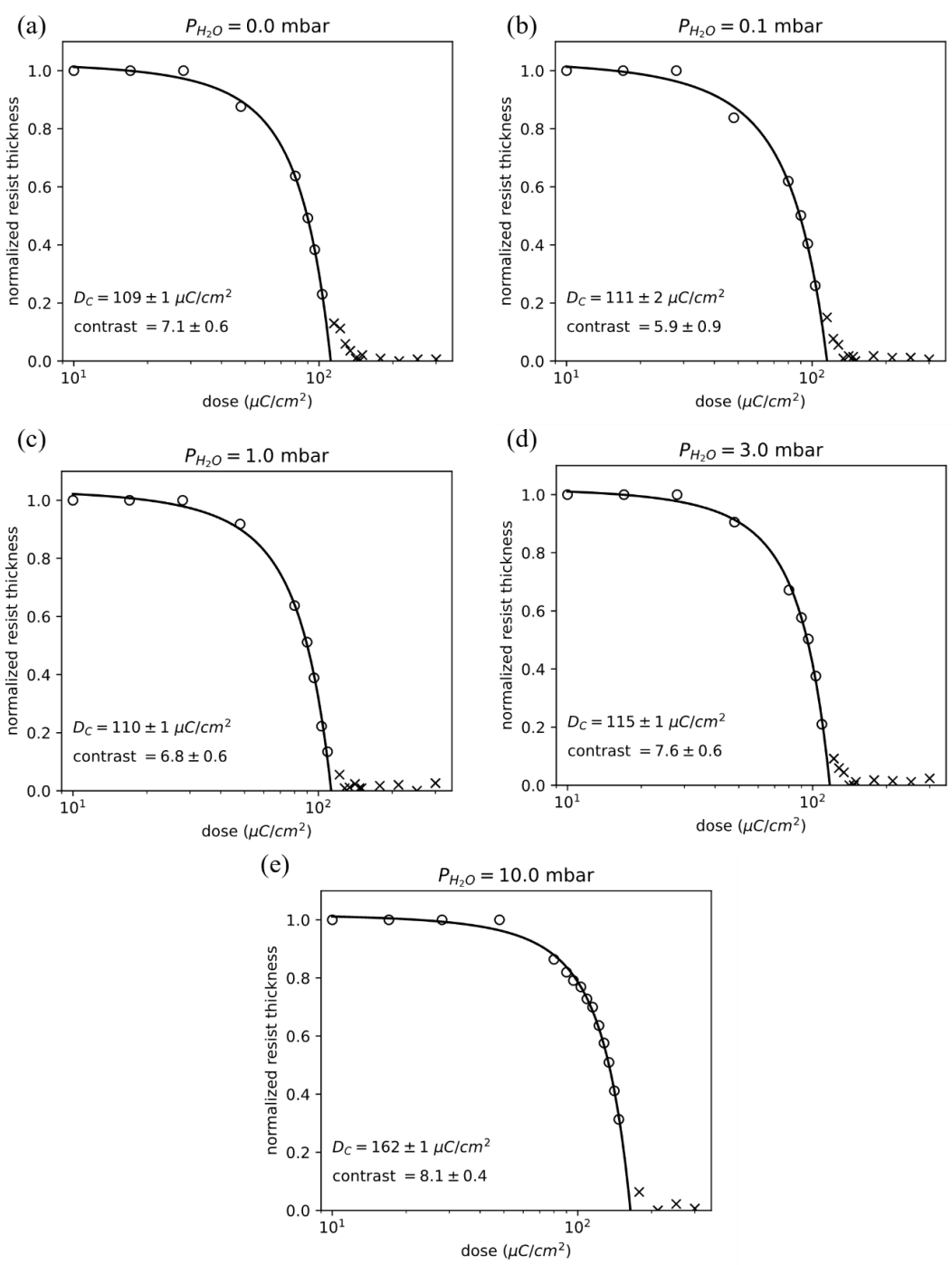

Figure 3. Fitted normalized resist thickness vs. exposure dose for each water vapor pressure used during resist exposure. (a) High vacuum; (b) 0.1 mbar; (c) 1 mbar; (d) 3 mbar and (e) 10 mbar. Data points used for the fit are indicated by a ○ while data points excluded from the fit are indicated by an ×. Dose to clear, D_C, and contrast for each dataset are shown inset. Uncertainties represent the standard error of the fitted parameter.

Table 2. Contrast (γ) and dose to clear (D_C) as a function of vapor pressure for positive tone exposure of PMMA.

Chamber Pressure	High Vacuum	0.1 mbar water vapor	1 mbar water vapor	3 mbar water vapor	10 mbar water vapor
Contrast	7.1 ± 0.6	5.9 ± 0.9	6.8 ± 0.6	7.6 ± 0.6	8.1 ± 0.4
Dose to clear ($\mu C/cm^2$)	109 ± 1	111 ± 2	110 ± 1	115 ± 1	162 ± 1

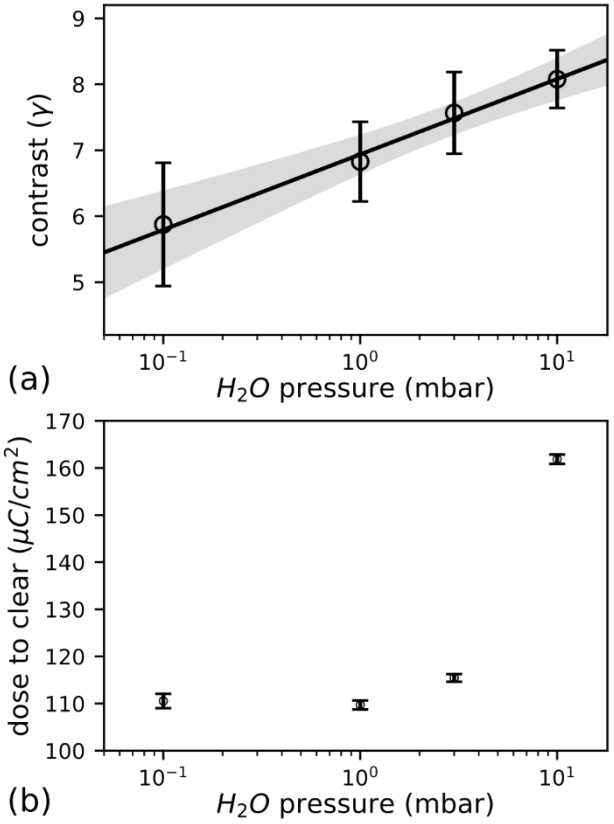

Figure 4. (a) Contrast as a function of water vapor pressure. The fitted line and corresponding 95% confidence bands (gray fill) show the statistically significant increase in contrast with vapor pressure. (b) Dose to clear as a function of water vapor pressure. The dose to clear increases sharply beyond 3 mbar. Error bars correspond to standard error of the fitted parameters.

2. *Infrared spectroscopy of positive-tone PMMA*

Infrared transmission spectra PMMA exposed under high vacuum and water vapor, as well as unexposed PMMA, were obtained to observe any changes in the chemical signature after exposure. Measurements were taken of undeveloped patterns exposed at 100 μC cm^{-2} and 175 μC cm^{-2}. The peaks present in unexposed PMMA and their respective mode assignments from infrared transmission data are summarized in Table 3.

Table 3 Vibrational mode assignments for PMMA from FTIR transmission data

Wavenumber (cm^{-1})		Modes[36,37]
3000	C-H	Asymmetric stretching
	$O-CH_3$	Asymmetric stretching
2952	$O-CH_3$	Symmetric stretching
	CH_2	Asymmetric stretching
	$C-CH_3$	Symmetric stretching
1730	C=O	Stretching
1483	CH_2	Bending
1450	C-H	Asymmetric bending
1435	C-H	Symmetric bending
1388	C-H	Symmetric bending
1272, 1242, 1193 and 1149	C-O-C	Stretching
989	$O-CH_3$	Rocking
842	CH_2	Rocking
750	C-C	Stretching

The infrared transmission spectra of PMMA irradiated at 175 μC cm^{-2} under high vacuum and water vapor (0.1 mbar, 1 mbar, 3 mbar and 10 mbar) are compared in Fig. 5 (a). Fig. 5 (b) shows infrared transmission spectra of unexposed PMMA and PMMA irradiated at 100 μC cm^{-2} under high vacuum and water vapor (0.1 mbar, 1 mbar, 3 mbar and 10 mbar). In both cases, the chemical signature of the irradiated patterns is not significantly altered for the dose range used for positive tone patterning. Furthermore, the presence of water vapor does not change the IR-active bonding. In the absence of chemical changes, alteration of the molecular weight distribution of the PMMA is the most likely explanation for the effect of water vapor on contrast.

Detailed studies of molecular weight distributions are beyond the scope of this work; however, one can readily identify radiation-chemical mechanisms associated with water radiolysis that would alter these distributions. Water radiolysis in environmental SEM, and subsequent beam damage to organic materials, is well established.[38–40] Likewise, enhanced etching of carbonaceous materials in water vapor has been observed for both electron beam[41] and ion beam[42–44] based processes. . Consider, for example, H· and ·OH radicals generated by water radiolysis. These radicals can abstract hydrogen from unexposed PMMA chains leading to unstable polymer radicals and subsequent main chain scission through mechanism (ii) in Fig. 1. Alternatively, these radicals can abstract hydrogen from polymer radicals previously generated by methyl ester cleavage. In this case, hydrogen abstraction would stabilize the polymer chain by mechanism (iv). Thus, depending on the relative abundance of polymer radicals and radiolysis products, the process could accelerate or slow main chain scission. Although atomic oxygen is not efficiently generated in hydrated samples,[38] it is expected in the vapor phase particularly in the presence of low-energy secondary electrons.[45–47] Atomic oxygen can directly react with PMMA chains to form volatile products, e.g. CO_2, which would reduce molecule weight. Complicating matters further, it is also

possible that the local water concentration is depleted by radiolysis, especially at higher doses. The details of how these processes compete to reduce contrast at lower vapor pressures and increase contrast at higher pressures are not currently understood. Establishing the details of the process will require extensive experiments and simulations to ascertain the reaction pathways along with the reaction rates among polymers chains, polymer radicals, and radiolysis products. However, simpler experiments that vary beam current, and thus dose rate, along with dwell and refresh times to study water depletion, may increase understanding of the underlying mechanism.

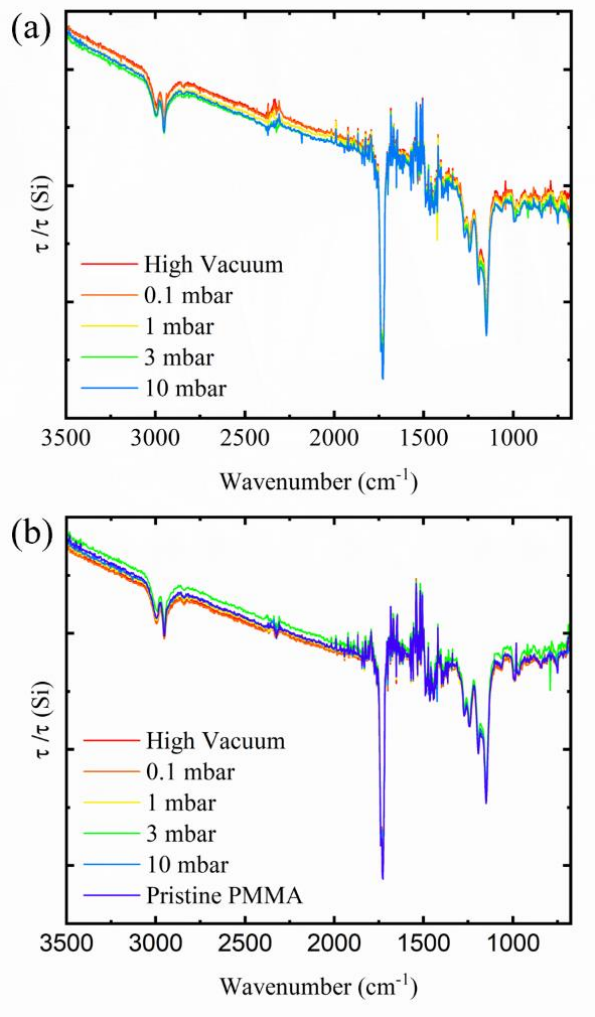

Figure 5. Infrared transmission spectra of (a) PMMA irradiated at 175 μC cm^{-2} under high vacuum and water vapor (0.1 mbar, 1 mbar, 3mbar and 10 mbar); (b) unexposed (pristine) PMMA and

PMMA irradiated at 100 μC cm^{-2} under high vacuum and water vapor (0.1 mbar, 1 mbar, 3mbar and 10 mbar)

B. Effect of water vapor on negative-tone patterning of PMMA

The decreased solubility of the exposed region in developer caused by the cross-linking of PMMA at higher exposure doses makes it function as a negative e-beam resist. Cross-linking among polymer chains leads to increased molecular weight of the resist. The widely accepted reaction mechanism suggests scission and cross-linking are not independent processes. Cross-linking occurs at sites that have previously undergone chain scission via path (i) of Fig. 1. The C=C bonding occurs at scissioned end groups leading to cross-linking.[48] The XPS results discussed below also suggest that additional linkages may form through C-O bonding.

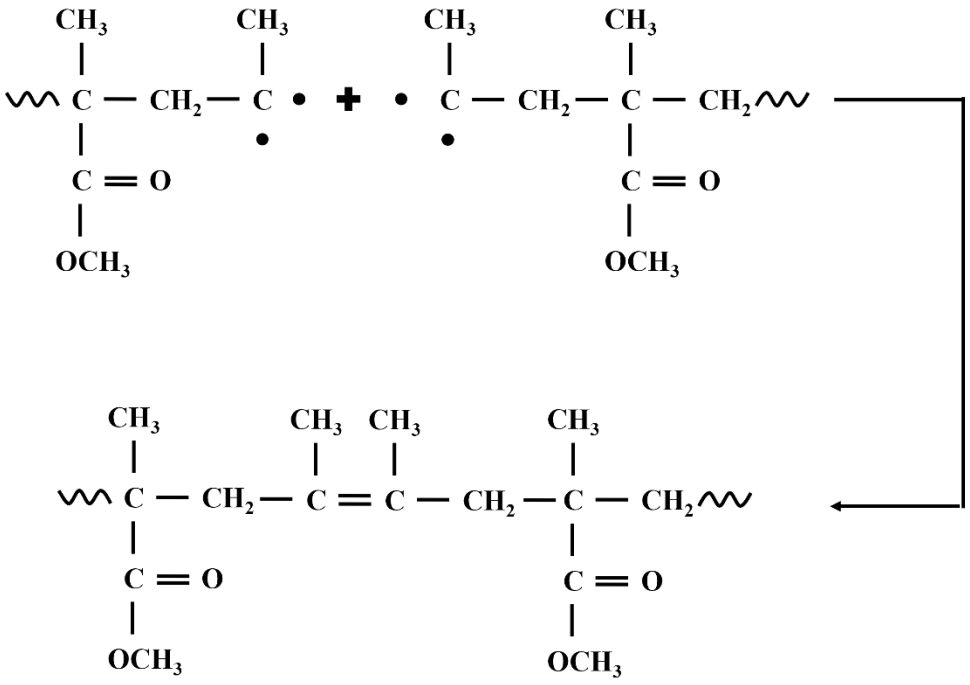

Figure 6. Reaction mechanism for main chain recombination resulting in crosslinking of the end groups[48]. Reproduced with permission from "E.M. Lehockey, I. Reid, and I. Hill, Journal of Vacuum Science & Technology A 6, 2221 (1988)." Copyright 1988 American Vacuum Society.

1. *Negative tone contrast curves*

Figure 7 shows the contrast curve for high-dose exposure of PMMA. The onset dose increases with increasing water vapor pressure. The final cross-linked resist thickness decreases with increasing water vapor pressure. This indicates that water-assisted e-beam induced etching of PMMA may significantly contribute to the process at these doses and pressures. The dose range used for these experiments was not sufficient to saturate the final resist thickness for 10 mbar water vapor exposure. Therefore, the normalized resist thickness and subsequent curve fitting has not been performed on 10 mbar water vapor data.

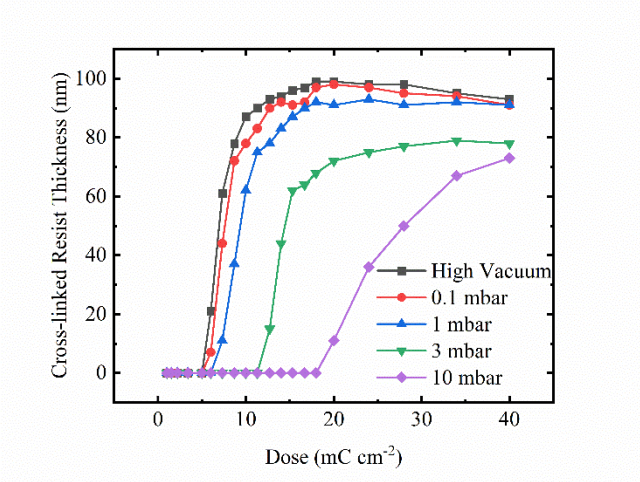

Figure 7. Contrast curves for higher exposure dose of array of 20 rectangles (5 µm x 50 µm). The exposure dose varied in the range of 1 mC cm^{-2} to 40 mC cm^{-2}.

For negative tone patterning, the normalized remaining resist thickness was fitted with an empirical model of the form

$$\mathrm{NRT} = C_0 - e^{S(D_O - D)} \qquad (4)$$

where the parameters are the same as the model in Eqn. (1) except that D_O represents the onset dose for negative-tone behavior. The fitted contrast curve for each water vapor pressure is shown

in Fig. 8 and Table 4 lists the contrast for each pressure. A drop in contrast, like that observed in the positive tone process, at 0.1 mbar water vapor was seen when compared to high vacuum exposure. The contrast increases at higher pressures as observed for positive tone behavior.

The cross-linking onset dose increases approximately linearly with water vapor pressure as shown in Fig. 9. The onset dose for crosslinking increases by a factor of 4 at 10 mbar water vapor as compared to high vacuum exposure. This large, approximately linear shift in onset dose is in stark contrast to the relatively small (~50%) and abrupt increase observed for dose to clear in positive tone patterning. Such a dramatic difference between positive and negative tone behavior cannot be explained by simple scattering of electrons in the water vapor. In the absence of compositional changes in the exposed materials, discussed below, these results again suggest that water vapor leads to a modification of the molecular weight, and molecular weight distribution, of exposed PMMA.

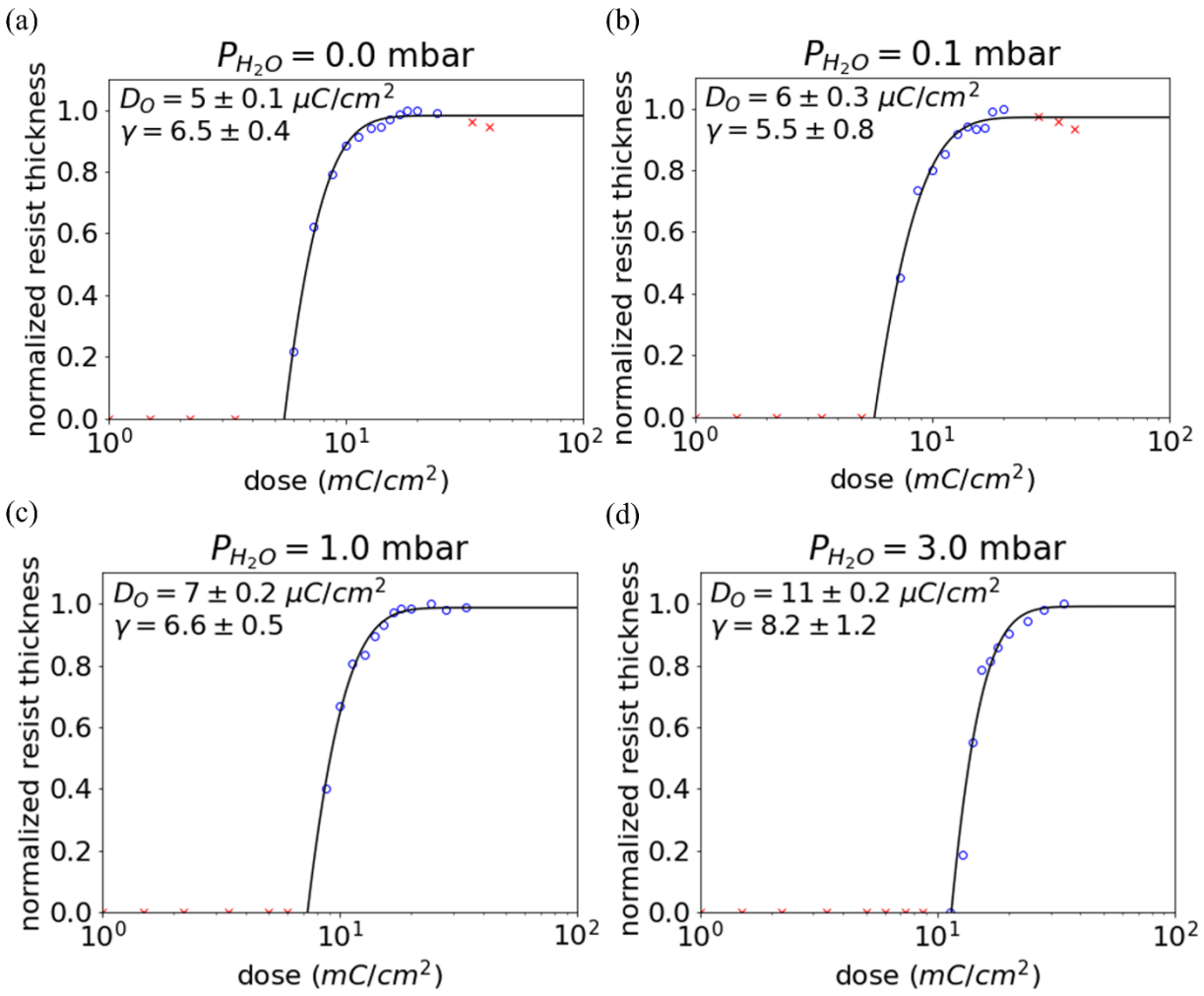

Figure 8 Normalized resist thickness (experimental and fitted) vs. exposure dose as a function of water vapor pressure: (a) High vacuum; (b) 0.1 mbar; (c) 1 mbar; and (d) 3 mbar. Onset dose, D_0, and contrast, γ, from the fitted model are shown for each water vapor pressure. Data points not well modeled by a standard contrast curve are excluded from the fit and indicated by an ×.

Table 4 Contrast (γ) as a function of vapor pressure for the negative tone behavior

Chamber Pressure	High Vacuum	0.1 mbar water vapor	1 mbar water vapor	3 mbar water vapor
Contrast (γ)	6.5 ± 0.4	5.5 ± 0.8	6.6 ± 0.5	8.2 ± 1.2

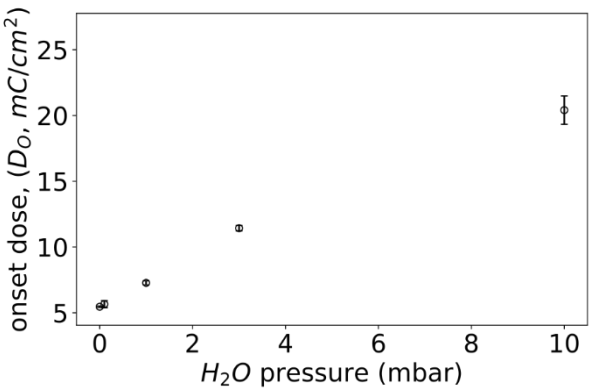

Figure 9. Onset dose for crosslinking as a function of water vapor pressure. Error bars represent standard error of the fit for the contrast curves.

Under vacuum and under water vapor, the thickness of cross-linked PMMA reaches a maximum just beyond the threshold for the negative tone behavior. The resist thickness decreases with increasing dose beyond threshold for high vacuum and 0.1 mbar water vapor pressure. The reduction in the final resist thickness with increasing dose, even in the absence of water vapor, suggests that compaction may be occurring at higher doses. In contrast to the positive tone process, a reduction in resist thickness was also noted before development at the doses required for negative tone behavior. Specifically, at 15 mC cm^{-2} during the negative tone process under high vacuum and 1 mbar water vapor, the PMMA thickness was reduced by 40% before development. Topography changes in PMMA before development upon irradiation has been widely reported in literature.[8,49–55] The film thickness decrease in the original material depends on the exposure method used.

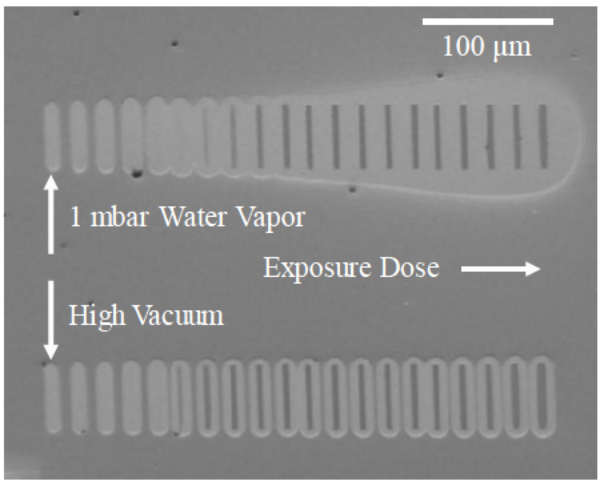

Figure 10. SEM image of 5 µm x 50 µm rectangular array structures exposed in the dose range 1 - 40 mC cm^{-2} under vacuum (lower pattern) and 1 mbar water vapor (upper pattern).

2. *VP-SEM as an alternative to large area positive tone writing*

Figure 10 shows the scanning electron microscopy (SEM) image of structures exposed in the dose range of 1 to 40 mC cm^{-2} under vacuum (lower pattern) and under 1 mbar water vapor (upper pattern). The exposure dose increases from left to right. It was observed that below the threshold of ~8 mC cm^{-2} PMMA retains the positive tone behavior where chain scission remains dominant mechanism, causing the first 5 rectangles of the pattern to completely clear under vacuum conditions. At exposure doses beyond 28 mC cm^{-2} an increase in the lateral dimensions of the developed pattern was observed. This is the result of the dose from backscattered electrons reaching the threshold for cross linking near the patterned structure.

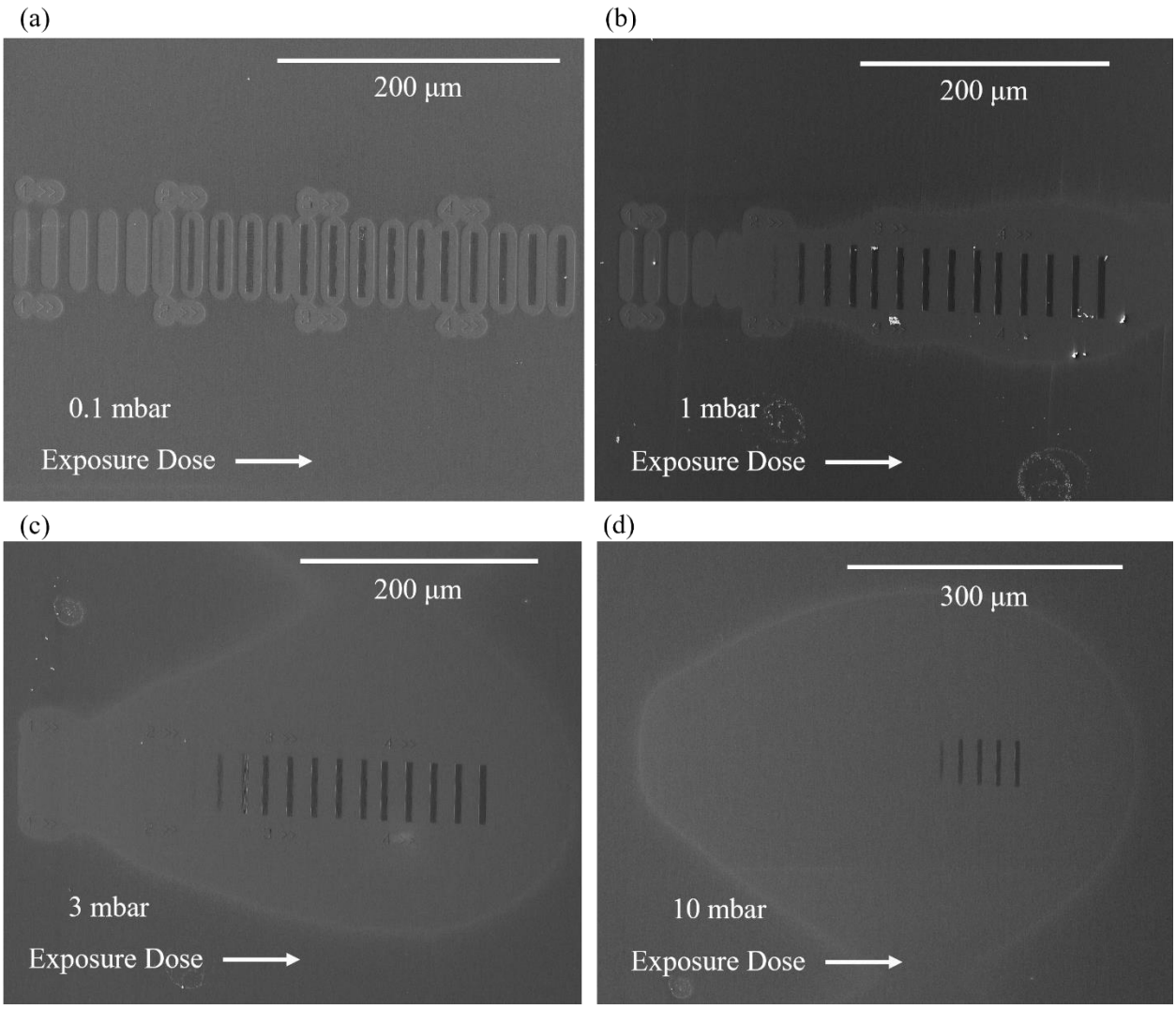

Figure 11 SEM images of patterns exposed in the dose range 1 - 40 mC cm^{-2} under (a) 0.1 mbar; (b) 1 mbar; (c) 3 mbar; and (d) 10 mbar water vapor. Exposure dose increases from left to right.

The threshold for cross-linking increases with increasing water vapor pressure, as is evident from the SEM images in Fig. 11. Figure 11 shows the SEM images for the same pattern, as shown in Fig. 10, exposed under identical conditions with increasing vapor pressure from (a) to (d). Additional features, numbers with arrow signs, seen in these SEM images were used as markers for AFM measurements. Other artifacts seen in the SEM images are gold nanoparticles that dispersed during development. Forward scattering in the water vapor yields a much larger clear

region around the negative-tone pattern with increasing vapor pressure. At higher water vapor pressures, the elastic scattering probability increases, thus an increase in the extent of the beam skirt with increasing gas scattering is observed.[27,56]

This effect could be useful for increasing the range of the developed region around cross-linked PMMA far beyond the backscattered electron range. Moreover, the range can be easily tuned by varying the water-vapor pressure. Thus, scattering in the water vapor can control the size of the cleared region around negative tone. This is advantageous compared to large area positive tone exposures around the negative tone pattern or attempting to control the size of the positive tone region by pre-exposure treatments such as vacuum drying.[57]

3. Infrared spectroscopy of negative-tone PMMA

Infrared transmission spectra were obtained for patterns irradiated at 15 mC cm^{-2} and 40 mC cm^{-2} under high vacuum and 1 mbar water vapor to better understand the exposure mechanism. In a previous study, it was found that exposure to an electron beam degrades the PMMA to produce molecular hydrogen, carbon monoxide and carbon dioxide.[8] The same study concluded that the methyl ester group in PMMA readily dissociates from the carbon backbone during irradiation. Figure 12 shows the comparison of transmission spectra under various conditions. High dose electron beam exposure causes the strong PMMA absorption peaks to broaden and weaken in irradiated samples. Features associated with the carboxyl and methoxy groups are weakened upon e-beam exposure, but the presence of water vapor during exposure does not significantly alter the spectrum.

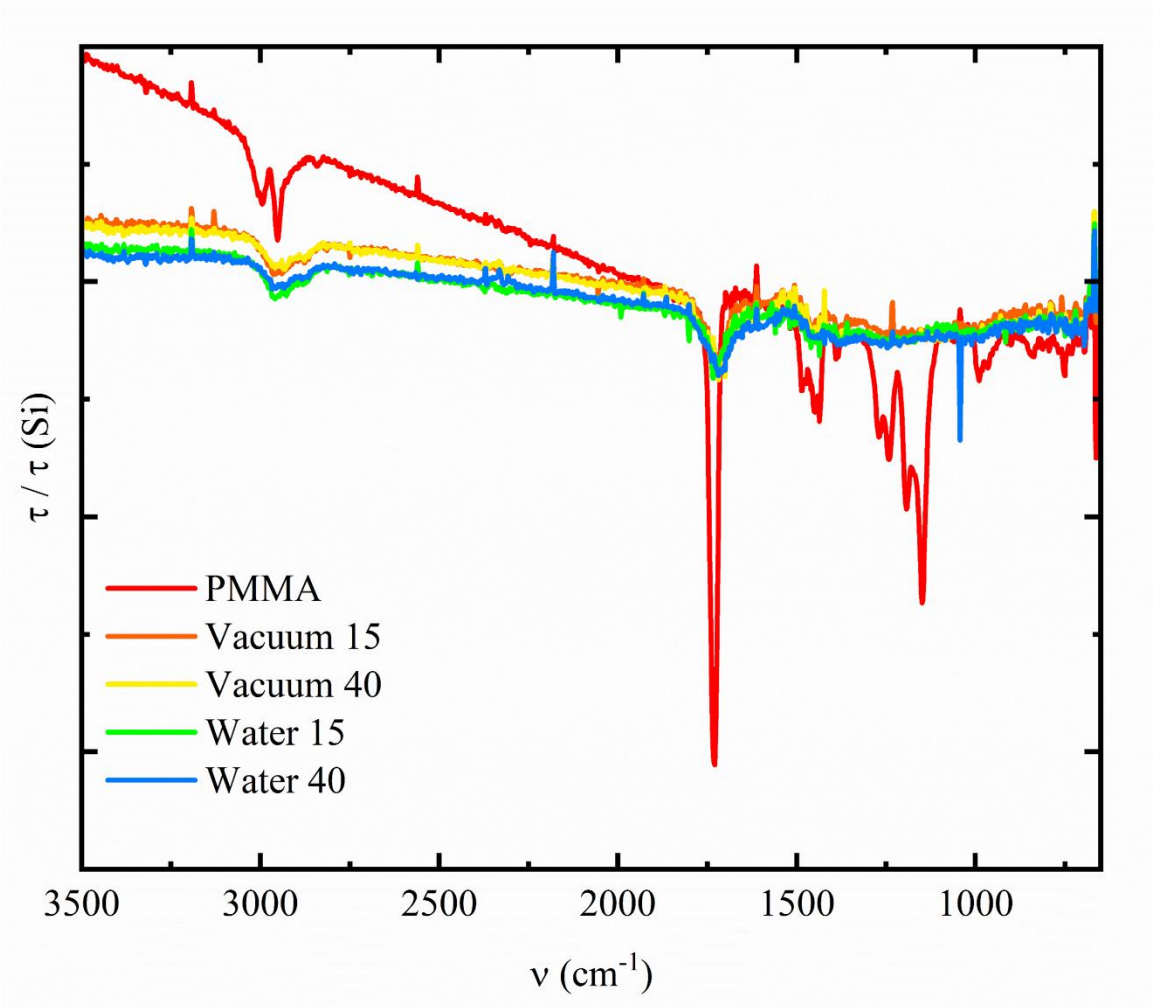

Figure 12. Infrared transmission spectra of PMMA unexposed (PMMA), exposed under 1 mbar water vapor, and exposed under high vacuum at 15 mC cm^{-2} (Water 15 and Vacuum 15) and 40 mC cm^{-2} (Water 40 and Vacuum 40). Features associated with the carboxyl and methoxy groups are weakened upon e-beam exposure, but the presence of water vapor during exposure does not significantly alter the spectrum.

The methoxy group (C-O-C stretching) peak 1149, 1193, 1242 and 1272 cm^{-1} lines disappears from the irradiated samples. The C=O stretching peak at 1730 cm^{-1} broadens and shifts to lower energies. This is consistent with the conversion of unconjugated C=O bonds to conjugated C=O bonds (which appear at lower wavenumbers[58]) upon irradiation. The C-H stretching absorption peak assigned to wavenumber 2952 cm^{-1} broadens as well whereas the C-H

stretching mode assigned to 3000 cm^{-1} disappears for irradiated samples. However, there was no significant difference observed for exposure under water vapor.

4. X-ray photoelectron spectroscopy of negative-tone PMMA

X-ray photoelectron spectroscopy (XPS) allows us to compare the chemical composition of unexposed PMMA with negative tone (cross-linked) PMMA exposed under high vacuum and water vapor. Here we use unexposed PMMA as a point of comparison and as a reference for establishing the binding energies and peak shapes of the relevant carbon-oxygen peaks. Subsequently, we use these parameters as a basis for fitting the XP spectra of exposed PMMA. In this way we can draw some basic conclusions about the chemical composition of the cross-linked PMMA and the effects of water vapor on the process.

For the C1s spectrum of unexposed PMMA, we assign four peaks to the five carbon atoms in the PMMA repeat unit as labeled in Figure 13(a). This approach was first proposed by Pijpers and Donners[59,60] and its chemical significance has been confirmed by several additional studies. (See, for example, references [61–64].) Peak fitting was performed with the following constraints: (1) A Shirely background was used that did not exceed the data at any point. (2) All peaks were modeled with a Gaussian-Lorentzian Sum (pseudoVoight) lineshape; (3) a single Gaussian-Lorentzian mixing ratio was fit for all peaks; (4) the relative binding energies were constrained to those given by Naves de Brito et al. for bulk PMMA,[61] and a single energy offset was fit to compensate for the small residual, charge-induced shift of the entire spectrum; (5) a single full width at half maximum (FWHM) was fit for all peaks as we do not have sufficient evidence that the intrinsic peak widths vary significantly for PMMA films more than a few nanometers thick;[62,63] and (6) the initial peak areas were chosen based on the stoichiometric concentrations,

but were allowed to vary without constraint because PMMA is known to exhibit slightly non-stoichiometric area ratios.[62]

Figure 13(a) shows the XP spectrum for unexposed PMMA, the Shirley background, the four fitted peaks, and the residual error in the fit. Table 5 lists the binding energies and compositional analysis results. This peak fitting strategy provided a good fit to the data and showed good agreement with other studies of bulk PMMA (see, for example, references [61,63]) including the slight non-stochiometric compositional results. Perhaps more importantly, these fits allowed us to confirm the binding energies and constrain the FWHM and mixing ratio for the peaks used to fit the XP spectra for exposed PMMA discussed below.

Table 5 XPS peak assignments and compositional analysis for unexposed PMMA. Uncertainties represent 95% confidence intervals for the fitted parameters. Parameters without uncertainties were fixed during the fit.

Label	Bonding	Binding Energy (eV)	Composition (at.%)
C1	CH_2 and CH_3	285.00 $\pm$0.01	43±1
C2	quaternary C	285.60	22 ±1
C3	O-CH_3	286.80	18.2±0.5
C4	O-C=O	289.00	16.5±0.3
All peaks: FWHM = 1.41±0.02 eV, Gaussian/Lorentzian mixing ratio = 0.16±0.02			

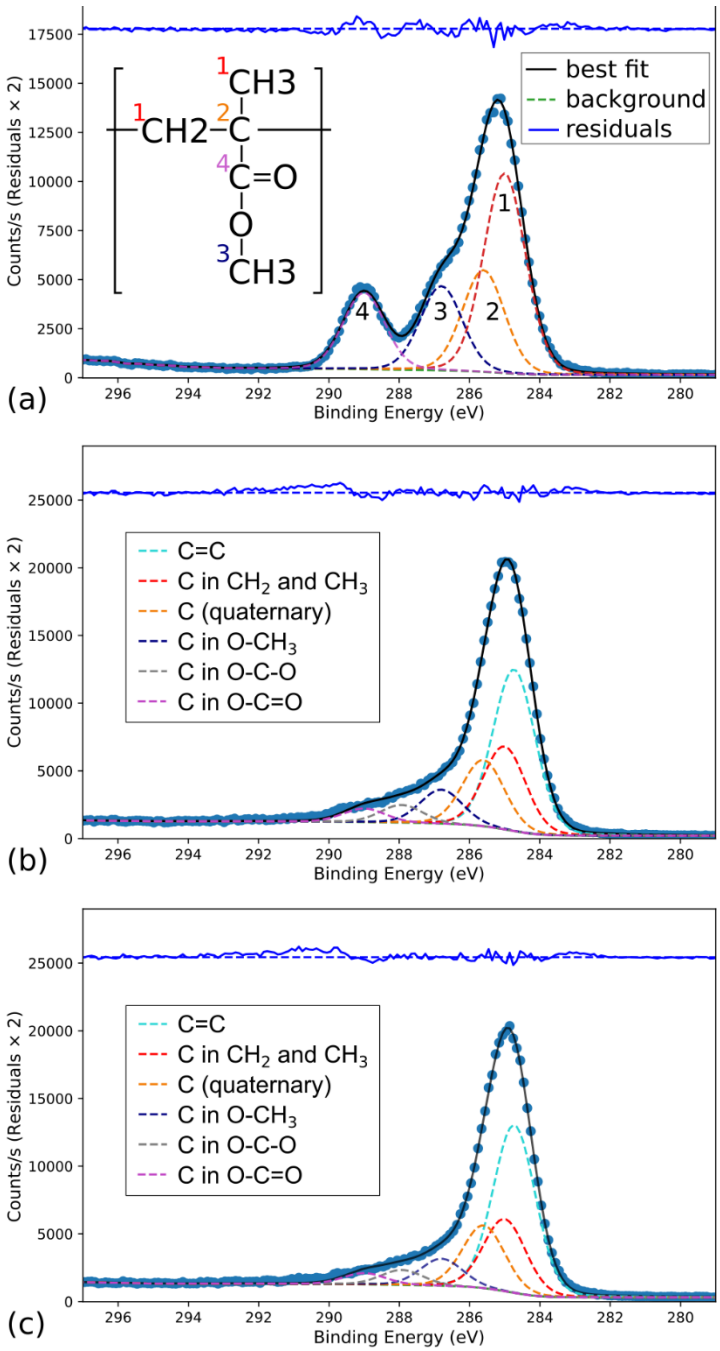

Figure 13. C1s X-ray photoelectron spectra for unexposed and negative-tone exposed PMMA. (a) Unexposed PMMA with polymer structure shown inset. The numerical labels on the fitted peaks indicate the associated carbon atom. (b) PMMA exposed under high vacuum. (c) PMMA exposed under 1 mbar water vapor. The exposure dose for (b) and (c) is 40 mC/cm^2. For (b) and (c) two additional peaks are included to capture the presence of C=C and O-C-O moieties.

Table 6 XPS peak assignments and compositional analysis for PMMA exposed at 40 mC/cm^2 under high vacuum and 1 mbar water vapor. Uncertainties represent 95% confidence intervals for the fitted parameters. Parameters without uncertainties were fixed during the fit.

Label	Bonding	Binding Energy (eV)	Composition for exposure under high vacuum (at.%)	Composition for exposure under 1 mbar water vapor (at.%)
	C=C	284.73	43±8	47±8
C1	CH_2 and CH_3	285.00±0.08	22±8	20±8
C2	quaternary C	285.60	18 ±1	18 ±1
C3	O-CH_3	286.80	9.0±0.4	7.6±0.4
	O-C-O	287.93	4.7±0.4	4.2±0.4
C4	O-C=O	289.00	3.6±0.3	3.2±0.3
All peaks: FWHM = 1.41 eV, Gaussian/Lorentzian mixing ratio = 0.16				

PMMA regions exposed with a dose of 40 mC/cm^2 under high vacuum and 1 mbar water vapor were also analyzed using XPS. The relative binding energies, FHWM, and mixing ratio from the unexposed PMMA were retained for the exposed PMMA analysis. However, prior studies have shown that cross-linked PMMA contains C=C bonds[48] and should have an additional peak shifted -0.27 eV from the C1 peak. In addition, none of the chemical shifts in unexposed PMMA account for the photoelectron signal near 288 eV in the cross-linked sample. Given the composition of PMMA, the only good candidate for this region is the carbon atom in O-C-O. We have added this peak based on the mean chemical shift (+2.93 eV) given by Gengenbach et al.[65] Naively fitting six peaks to the relatively smooth spectrum of cross-linked PMMA would be quite challenging and would lead to unacceptably large uncertainties for the peak parameters and the composition of the material. However, by retaining the relative binding energies, FWHM, and

mixing ratio from unexposed PMMA measured at the same time and on the same substrate, we can sufficiently constrain the fit to draw some meaningful conclusions.

Figure 13(b) and (c) show the XP spectra for PMMA exposed under high vacuum and water vapor respectively. The Shirley background, the six fitted peaks, and the residual error in the fit as shown as well. Table 6 lists the binding energies and compositional analysis results. With regard to composition, it comes as no surprise that the area of the C=C peak is strongly negatively correlated with the area of the adjacent C1 peak associated with CH_2 and CH_3. This leads to substantial uncertainty in the relative compositions. Nevertheless, the confidence intervals exclude a zero concentration of C=C even at the 99.73% confidence level. Thus, our results reaffirm the conclusion of prior works, sometimes reported without measures of uncertainty, that cross-linking of PMMA occurs at least partially through C=C bonds. This result is also consistent with the infrared spectroscopy results of Section III.B.3 which shows the transformation of unconjugated C=O bonds to conjugated C=O bonds after irradiation at similar doses.

The distinct shoulder and higher energy peak associated with C3 and C4 respectively are markedly reduced upon irradiation. Neither result is surprising as side-group cleavage accompanies main chain scission in electron-exposure of PMMA. More interesting is the photoelectron signal that appears to arise from O-C-O bonded carbon. Excluding this moiety significantly reduced the quality of the fit, and the confidence intervals for the area of the O-C-O peak exclude zero concentration even at the 99.73% confidence level. This suggests that cross-linking can also occur through a more complex linkage involving oxygen. Based on the spectra of acetal/ketal linkages, we would expect additional infrared absorption in the 1200-1010 cm^{-1} range. However, it would be difficult to detect the four to five unresolved features expected for such O-C-O linkages[58] in the infrared spectra of Figure 12. This is especially true given the low

concentration identified by XPS. Thus, this observation should motivate further study to fully characterize the various cross-linking mechanisms for negative-tone PMMA.

These results add additional insight into the cross-linking process for negative-tone PMMA exposure beyond what has been previously presented in the literature. However, the most important result for this study is that there are only very small chemical differences between negative tone PMMA exposed under 1 mbar water vapor and PMMA exposed under high vacuum. The carbon-carbon bonded components (C1, C2, and C=C) do not shown any statistically significant difference at the 95% confidence level. Among the carbon-oxygen bonded components, only C3 shows a small statistically significant compositional difference (1.4%). As noted above, these results are consistent with our infrared spectra which also shows only very small chemical differences between negative-tone exposure under vacuum and water vapor. This result contrasts with reported changes in PMMA composition during ion-beam etching using large argon ion clusters with and without water vapor. In the case of ion-beam etching, XPS showed water vapor reduced the loss of C-O and O-C=O bonded carbon compared to irradiation in vacuum.[66] Even so, argon ion cluster experiments represent a vastly different regime of total dose, dose rate, and localization of energy transfer.

Thus, X-ray photoelectron and infrared spectroscopy both suggest that water vapor does not change the composition of the cross-linked PMMA. Thus, compositional changes are not likely the source of the enhanced contrast and the dramatic change in onset dose observed for exposure under water vapor. Rather, reactions with water radiolysis products, as discussed in Section III.A.1, may alter the molecular weight and molecular weight distributions.

IV. SUMMARY AND CONCLUSIONS

Water vapor was recently shown to alter the radiation chemistry of the VP-EBL process for Teflon AF[26]. In this work, VP-EBL was conducted to study the effect of water vapor on positive and negative tone electron-beam patterning of PMMA, a conventional e-beam resist. Water vapor did not dramatically affect the sensitivity of PMMA for the positive tone patterning at vapor pressures up to 3 mbar. However, the contrast of the positive and the negative tone process improved in the presence of water vapor. These results suggest that VP-EBL can be applied to positive-tone patterning PMMA without extensive changes to established process parameters. In contrast, water vapor dramatically increased the onset dose for negative tone patterning and both compaction and direct etching appear to be significant. Improved contrast was also observed for negative-tone patterning at higher water vapor pressures. As a result, significant process modifications will be necessary when implementing VP-EBL for negative tone PMMA patterning.

X-ray photoelectron spectra and infrared transmission spectra indicate that the presence of water vapor does not dramatically alter the composition of exposed PMMA. This is true for both positive and negative tone processes. Instead, changes in molecular weight distributions appear to be responsible for the altered contrast and contribute to the changes in clearing and onset dose. Further investigation is required to establish the radiation chemical mechanisms, such as hydrogen a st raction y H· and ·OH, that can alter the chain scission and cross-linking processes and thus the molecular weight distributions.

Finally, scattering in the water vapor can control the size of the cleared region around negative tone patterns providing an alternative to large area positive tone writing to achieve the same end. This effect could be useful for increasing the range of the developed region around cross-linked PMMA far beyond the backscattered electron range. Moreover, the range can be

easily tuned by varying the water-vapor pressure. All of these results emphasize the dramatic expansion of the lithographic parameter space when conducting electron-beam lithography under reactive gases.

ACKNOWLEDGMENTS

This material is based upon work supported by the National Science Foundation under Grant No. CMMI-2135666. This work was performed in part at the University of Kentucky Center for Nanoscale Science and Engineering and Electron Microscopy Center, members of the National Nanotechnology Coordinated Infrastructure (NNCI), which is supported by the National Science Foundation (NNCI-2025075).

AUTHOR DECLARATIONS

Conflict of Interest

The authors have no conflicts to disclose.

DATA AVAILABILITY

The data that support the findings of this study are available from the corresponding author upon reasonable request.

REFERENCES

[1] H.M. Lee, Y.N. Kim, B.H. Kim, S.O. Kim, and S.O. Cho, Advanced Materials **20**, 2094 (2008).

[2] C.A. Barrios, S. Carrasco, V. Canalejas-Tejero, D. López-Romero, F. Navarro-Villoslada, M.C. Moreno-Bondi, J.L.G. Fierro, and M.C. Capel-Sánchez, Mater. Lett. **88**, 93 (2012).

[3] A.M. Tatara, S.R. Shah, M. Sotoudeh, A.M. Henslee, M.E. Wong, A. Ratcliffe, F. Kurtis Kasper, and A.G. Mikos, J. Med. Devices **9(2): 024501** (2015).

[4] N. Zheng, H. Min, Y. Jiang, and X. Cheng, J. Vac. Sci. Technol. B **36**, 021603 (2018).

[5] F. Zheng, Y. Zhang, J. Xia, C. Xiao, and Z. An, Journal of Applied Physics **106**, 064105 (2009).

[6] A. Gangnaik, Y.M. Georgiev, B. McCarthy, N. Petkov, V. Djara, and J.D. Holmes, Microelectron. Eng. **123**, 126 (2014).

[7] T.-Y. Chung, D. Nest, D.B. Graves, F. Weilnboeck, R.L. Bruce, G.S. Oehrlein, D. Wang, M. Li, and E.A. Hudson, J. Phys. D: Appl. Phys. **43**, 272001 (2010).

[8] C.P. Ennis and R.I. Kaiser, Phys. Chem. Chem. Phys. **12**, 14902 (2010).

[9] J.J. Ritsko, L.J. Brillson, R.W. Bigelow, and T.J. Fabish, J. Chem. Phys. **69**, 3931 (1978).

[10] N.L. Mathakari, V.N. Bhoraskar, and S.D. Dhole, Mater. Sci. Eng. B - Adv. **168**, 122 (2010).

[11] T. Sasuga, N. Hayakawa, K. Yoshida, and M. Hagiwara, Polymer **26**, 1039 (1985).

[12] S.O. Cho and H.Y. Jun, Nucl. Instrum. Meth. B **237**, 525 (2005).

[13] M. Sabet, A. Hassan, and C.T. Ratnam, Polym. Bull. **68**, 2323 (2012).

[14] Y.K. Hong, D.H. Park, S.K. Park, H. Song, D.-C. Kim, J. Kim, Y.H. Han, O.K. Park, B.C. Lee, and J. Joo, Adv. Funct. Mater. **19**, 567 (2009).

[15] R.P. Oleksak, R.E. Ruther, F. Luo, K.C. Fairley, S.R. Decker, W.F. Stickle, D.W. Johnson, E.L. Garfunkel, G.S. Herman, and D.A. Keszler,ACS Appl. Mater. Interfaces, 6, 2917−2921 (2014).

[16] B. Bita, E. Stancu, D. Stroe, M. Dumitrache, S.C. Ciobanu, S.L. Iconaru, D. Predoi, and A. Groza, Polymers (Basel) **14**, 582 (2022).

[17] B.-R. Lu, M. Lanniel, M. Alexandar, R. Liu, Y. Chen, and E. Huq, J. Vac. Sci. Technol. B **29**, 030604 (2011).

[18] T. Maeno, T. Futami, H. Kushibe, and T. Takada, Journal of Applied Physics **65**, 1147 (1989).

[19] M. Hatzakis, J. Electrochem. Soc. **116**, 1033 (1969).

[20] I. Zailer, J.E.F. Frost, V. Chabasseur-Molyneux, C.J.B. Ford, and M. Pepper, Semicond. Sci. Technol. **11**, 1235 (1996).

[21] H. Duan, D. Winston, J.K.W. Yang, B.M. Cord, V.R. Manfrinato, and K.K. Berggren, J. Vac. Sci. Technol. B **28**, C6C58 (2010).

[22] T.M. Hall, A. Wagner, and L.F. Thompson, Journal of Applied Physics **53**, 3997 (1982).

[23] A.N. Broers, J.M.E. Harper, and W.W. Molzen, Appl. Phys. Lett. **33**, 392 (1978).

[24] A.C.F. Hoole, M.E. Welland, and A.N. Broers, Semicond. Sci. Technol. **12**, 1166 (1997).

[25] B.D. Myers and V.P. Dravid, Nano Letters **6**, 963 (2006).

[26] M.A. Sultan, S.K. Lami, A. Ansary, D.R. Strachan, J.W. Brill, and J.T. Hastings, Nanotechnology **30**, 305301 (2019).

[27] A. Zoukel, L. Khouchaf, J.Di. Martino, and D. Ruch, Micron **44**, 107 (2013).

[28] D.E. Newbury, J Res Natl Inst Stand Technol **107**, 567 (2002).

[29] M. Newville, T. Stensitzki, D.B. Allen, and A. Ingargiola, (2014).

[30] J.O. Choi, J.A. Moore, J.C. Corelli, J.P. Silverman, and H. Bakhru, J. Vac. Sci. Technol. B: Microelectronics Processing and Phenomena **6**, 2286 (1988).

[31] H. Hiraoka, IBM Journal of Research and Development **21**, 121 (1977).

[32] V.M. Bermudez, J. Vac. Sci. Technol. B: Microelectronics and Nanometer Structures Processing, Measurement, and Phenomena **17**, 2512 (1999).

[33] L.E. Ocola, M. Costales, and D.J. Gosztola, Nanotechnology **27**, 035302 (2015).

[34] G.D. Danilatos, in Adv. Electron. El. Phys., edited by P.W. Hawkes (Academic Press, 1988), pp. 109–250.

[35] B. Myers, Z. Pan, and V. Dravid, Microsc Microanal **14**, 1208 (2008).

[36] H.A. Willis, V.J.I. Zichy, and P.J. Hendra, Polymer **10**, 737 (1969).

[37] S. Dirlikov and J.L. Koenig, Appl. Spectrosc., AS **33**, 551 (1979).

[38] C.P. Royall, B.L. Thiel, and A.M. Donald, J Microsc **204**, 185 (2001).

[39] Kitching and Donald, Journal of Microscopy **190**, 357 (1998).

[40] L.M. Jenkins and A.M. Donald, Scanning **19**, 92 (1997).

[41] P.S. Spinney, D.G. Howitt, S.D. Collins, and R.L. Smith, Nanotechnology **20**, 465301 (2009).

[42] T.J. Stark, G.M. Shedd, J. Vitarelli, D.P. Griffis, and P.E. Russell, J. Vac. Sci. Technol. B: Microelectronics and Nanometer Structures Processing, Measurement, and Phenomena **13**, 2565 (1995).

[43] T.J. Stark, D.P. Griffis, and P.E. Russell, J. Vac. Sci. Technol. B: Microelectronics and Nanometer Structures Processing, Measurement, and Phenomena **14**, 3990 (1996).

[44] I. Utke, P. Hoffmann, and J. Melngailis, J. Vac. Sci. Technol. B: Microelectronics and Nanometer Structures Processing, Measurement, and Phenomena **26**, 1197 (2008).

[45] O.P. Makarov, J.M. Ajello, P. Vattipalle, I. Kanik, M.C. Festou, and A. Bhardwaj, J. Geophys. Res. - Space **109**, (2004).

[46] R. Monckton, Low-energy Electron Interactions with Water, PhD Thesis, University of Manchester, Manchester, (2014).

[47] T. Ogawa, N. Yonekura, M. Tsukada, S. Ihara, T. Yasuda, H. Tomura, K. Nakashima, and H. Kawazumi, J. Phys. Chem. **95**, 2788 (1991).

[48] E.M. Lehockey, I. Reid, and I. Hill, J. Vac. Sci. Technol. A **6**, 2221 (1988).

[49] W. Hong, H.-J. Woo, H.-W. Choi, Y.-S. Kim, and G. Kim, Applied Surface Science **169–170**, 428 (2001).

[50] S.J. Erasmus, J. Vac. Sci. Technol. B: Microelectronics Processing and Phenomena **5**, 409 (1987).

[51] T. Borzenko, A. Vyatkin, N. Gonchakova, V. Zinenko, Y.I. Koval, and V. Kudryashov, Vacuum **38**, 1007 (1988).

[52] J.C. Shaw, S.A. Rishton, R.R. Jackson, and M.P. O'Boyle, Appl. Phys. Lett. **58**, 310 (1991).

[53] J.T. Woodward, K.-W. Choi, V.M. Prabhu, S. Kang, K.A. Lavery, W. Wu, M. Leeson, A.D. Silva, N.M. Felix, and C.K. Ober, in *Advances in Resist Materials and Processing Technology XXV* (SPIE, 2008), pp. 720–731.

[54] E.A. Dobisz, J. Vac. Sci. Technol. B **15**, 2318 (1997).

[55] E.A. Dobisz, S.L. Brandow, R. Bass, and L.M. Shirey, J. Vac. Sci. Technol. B: Microelectronics and Nanometer Structures Processing, Measurement, and Phenomena **16**, 3695 (1998).

[56] E. Doehne and N. Bower, Microbeam Analysis **2**, S35 (1993).

[57] A.F.G. Leontowich, A.P. Hitchcock, T. Tyliszczak, M. Weigand, J. Wang, and C. Karunakaran, J Synchrotron Rad **19**, 976 (2012).

[58] D.L. Pavia, G.M. Lampman, G.S. Kriz, and J.R. Vyvyan, *Introduction to Spectroscopy*, Fifth edition (Cengage Learning, Stamford, CT, 2015).

[59] A.P. Pijpers and W. a. B. Donners, Journal of Polymer Science: Polymer Chemistry Edition **23**, 453 (1985).

[60] A.P. Pijpers and W. a. B. Donners, J. Polym. Sci. Pol. Lett. **24**, 653 (1986).

[61] A. Naves de Brito, M.P. Keane, N. Correia, S. Svensson, U. Gelius, and B.J. Lindberg, Surf. Interface Anal. **17**, 94 (1991).

[62] G. Beamson, A. Bunn, and D. Briggs, Surf. Interface Anal. **17**, 105 (1991).

[63] P. Louette, F. Bodino, and J.-J. Pireaux, Surface Science Spectra **12**, 69 (2005).

[64] C. Girardeaux and J.-J. Pireaux, Surface Science Spectra **4**, 134 (1996).

[65] T.R. Gengenbach, G.H. Major, M.R. Linford, and C.D. Easton, J. Vac. Sci. Technol. A **39**, 013204 (2021).

[66] N. Toyoda and I. Yamada, Appl. Surf. Sci. **310**, 112 (2014).

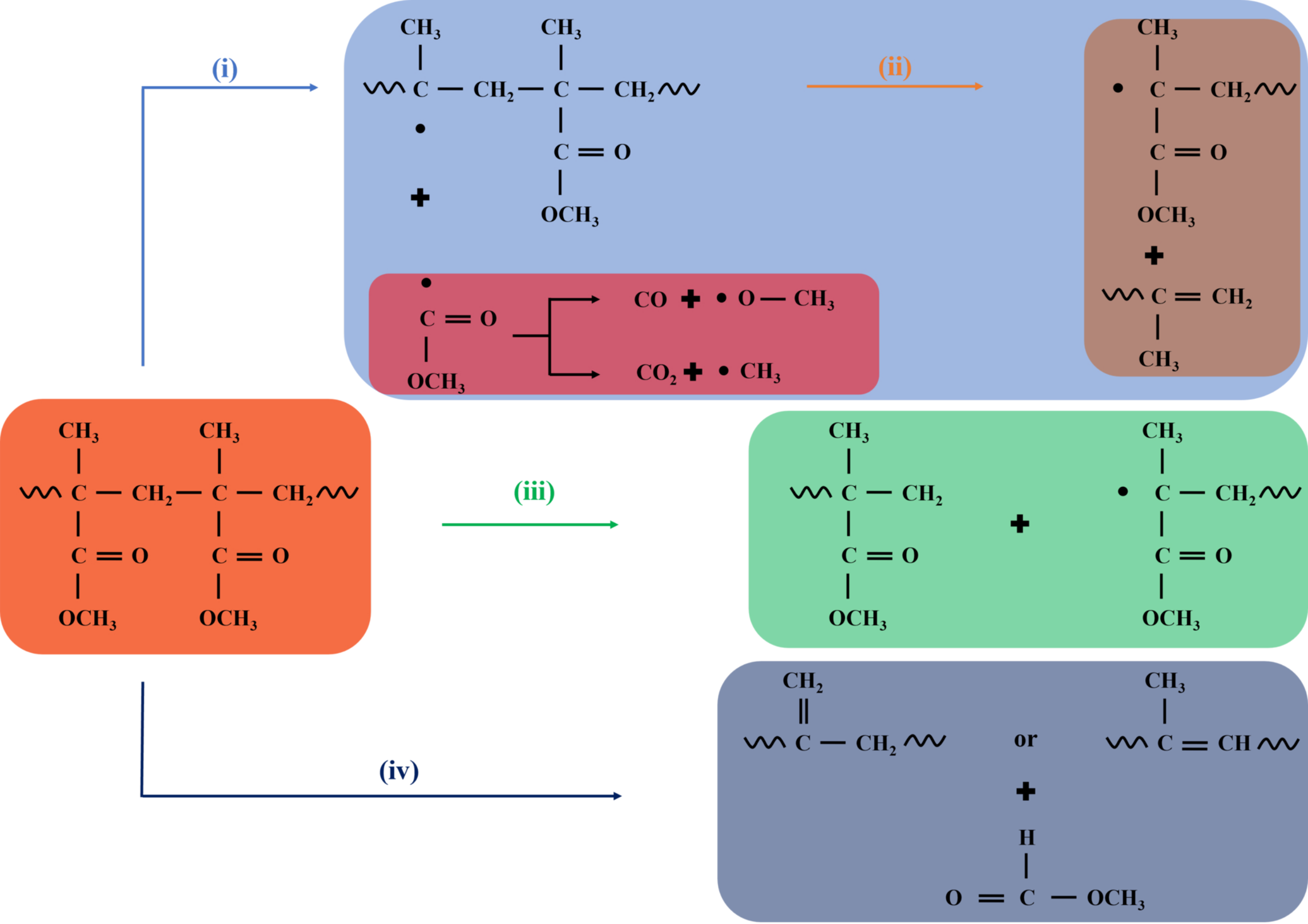
(i)
(ii)
(iii)
(iv)
CO + • O — CH3
CO2 + • CH3
or

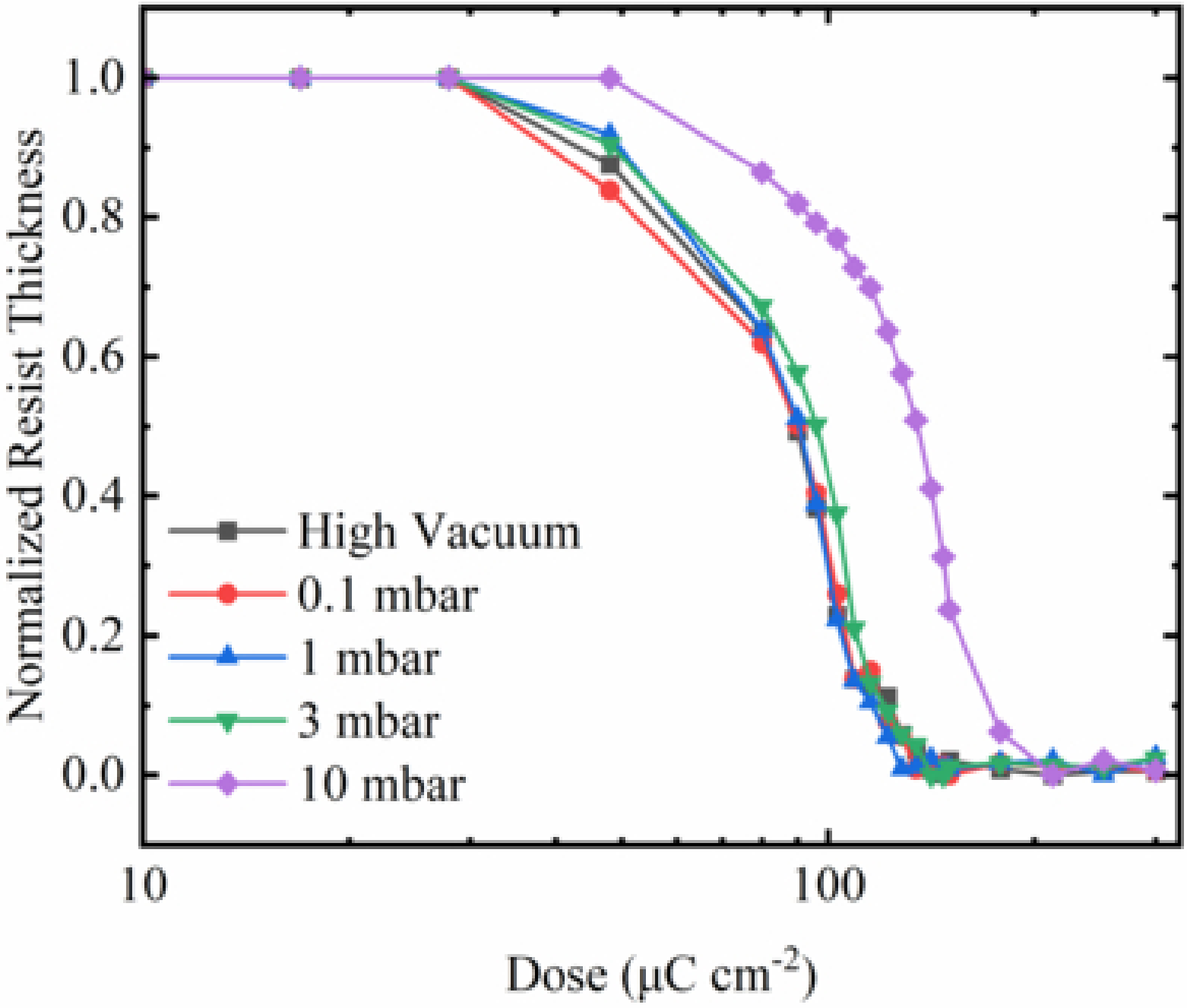
Normalized Resist Thickness
1.0
0.8
0.6
0.4
0.2
0.0
High Vacuum
0.1 mbar
1 mbar
3 mbar
10 mbar
10
100
Dose (μC cm-2)

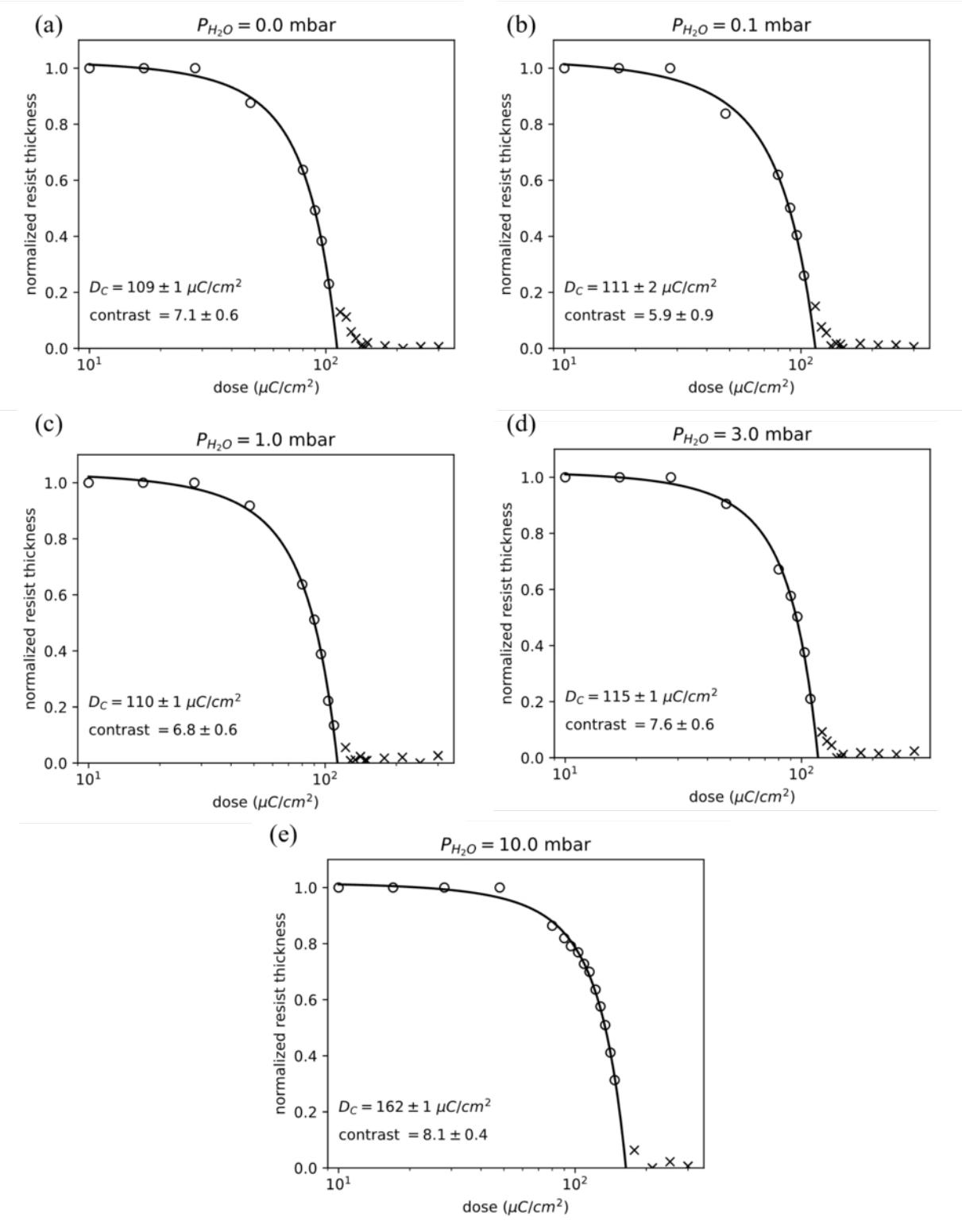
(a)
$P_{H_2O} = 0.0$ mbar
normalized resist thickness
dose ($\mu C/cm^2$)
$D_C = 109 \pm 1\ \mu C/cm^2$
contrast $= 7.1 \pm 0.6$
(b)
$P_{H_2O} = 0.1$ mbar
normalized resist thickness
dose ($\mu C/cm^2$)
$D_C = 111 \pm 2\ \mu C/cm^2$
contrast $= 5.9 \pm 0.9$
(c)
$P_{H_2O} = 1.0$ mbar
normalized resist thickness
dose ($\mu C/cm^2$)
$D_C = 110 \pm 1\ \mu C/cm^2$
contrast $= 6.8 \pm 0.6$
(d)
$P_{H_2O} = 3.0$ mbar
normalized resist thickness
dose ($\mu C/cm^2$)
$D_C = 115 \pm 1\ \mu C/cm^2$
contrast $= 7.6 \pm 0.6$
(e)
$P_{H_2O} = 10.0$ mbar
normalized resist thickness
dose ($\mu C/cm^2$)
$D_C = 162 \pm 1\ \mu C/cm^2$
contrast $= 8.1 \pm 0.4$

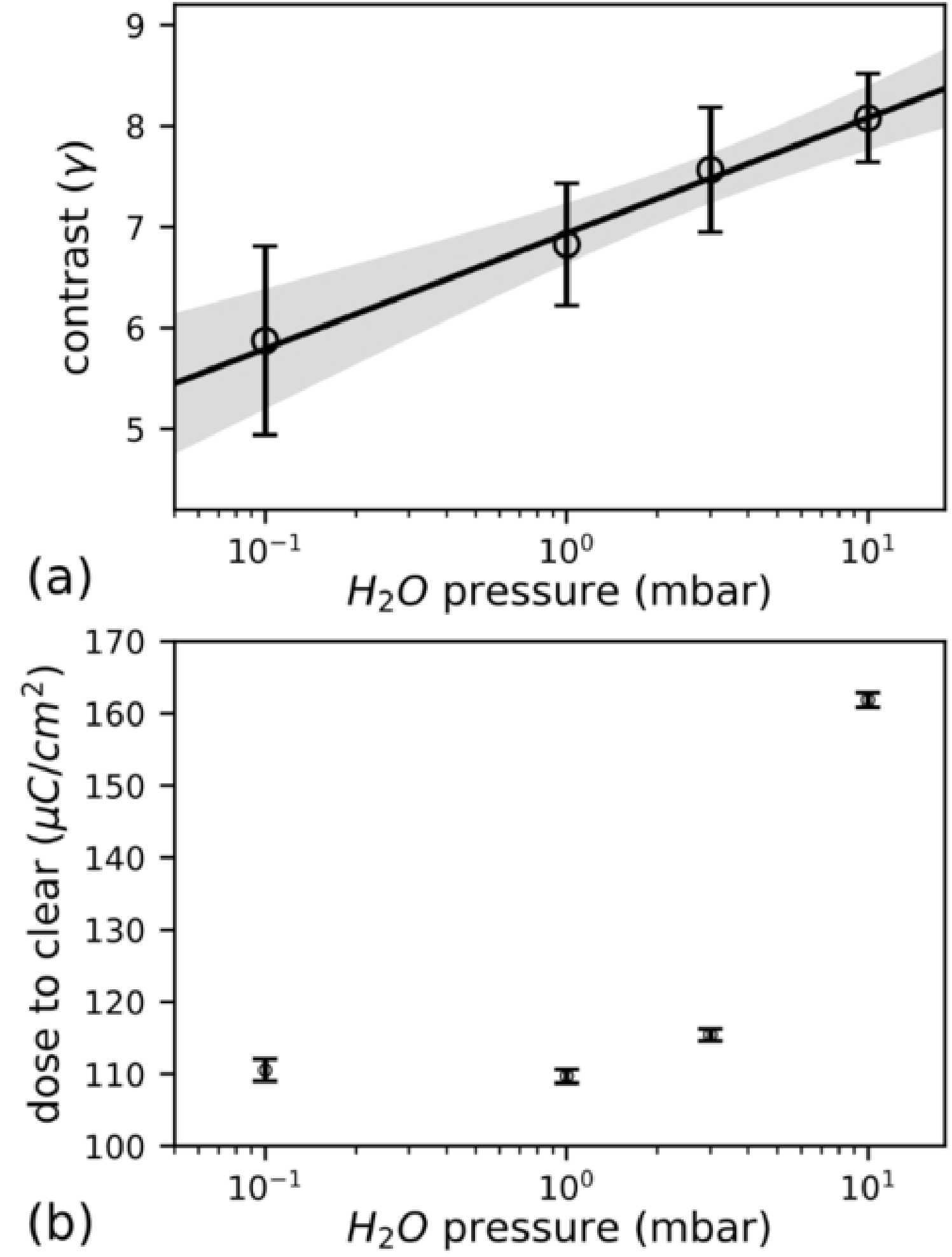
contrast (γ)
9
8
7
6
5
10^{-1}
10^{0}
10^{1}
H_2O pressure (mbar)
(a)
dose to clear ($\mu C/cm^2$)
170
160
150
140
130
120
110
100
10^{-1}
10^{0}
10^{1}
H_2O pressure (mbar)
(b)

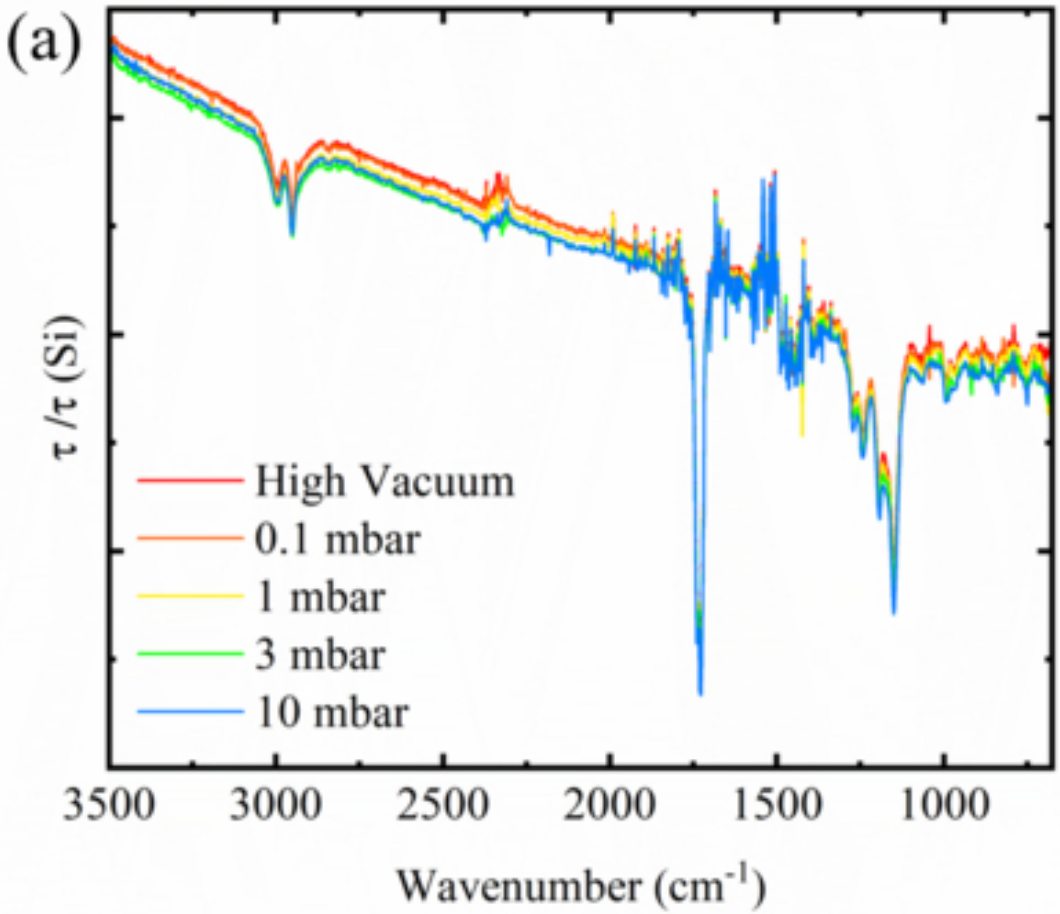
(a)
τ /τ (Si)
High Vacuum
0.1 mbar
1 mbar
3 mbar
10 mbar
3500
3000
2500
2000
1500
1000
Wavenumber (cm-1)

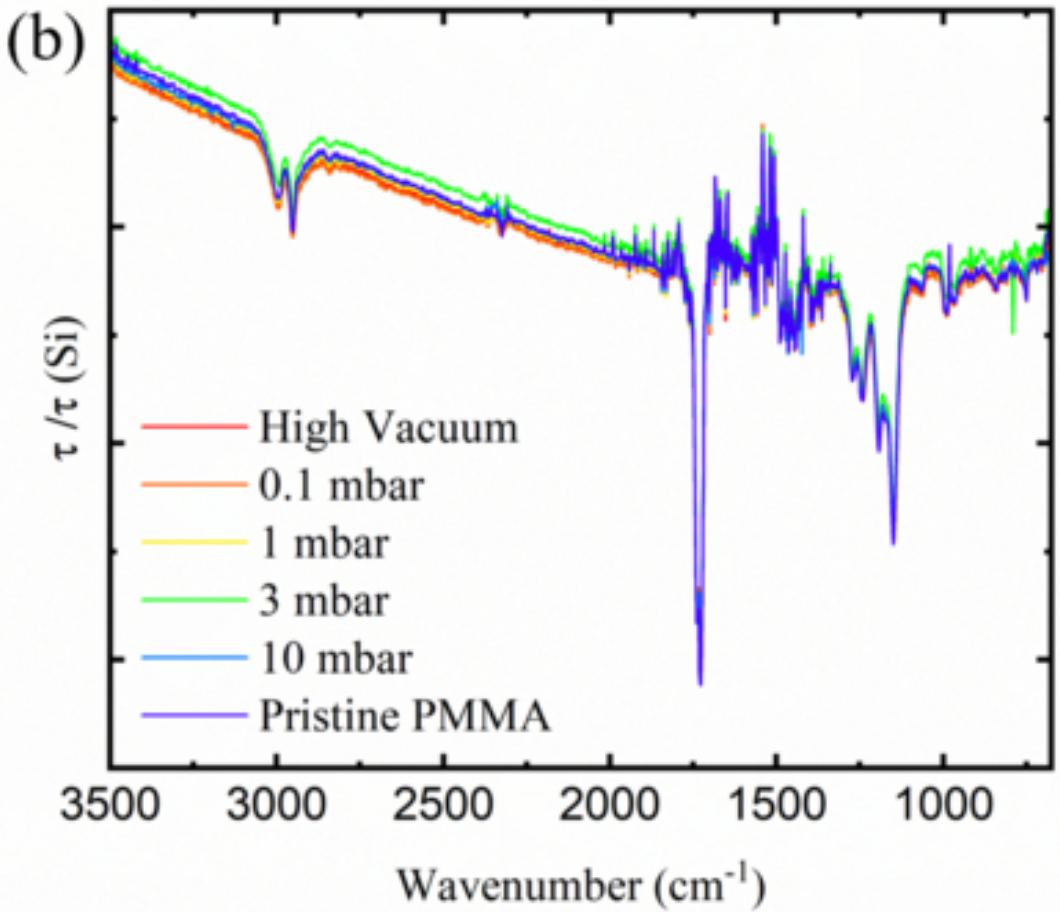
(b)
τ /τ (Si)
High Vacuum
0.1 mbar
1 mbar
3 mbar
10 mbar
Pristine PMMA
3500
3000
2500
2000
1500
1000
Wavenumber (cm-1)

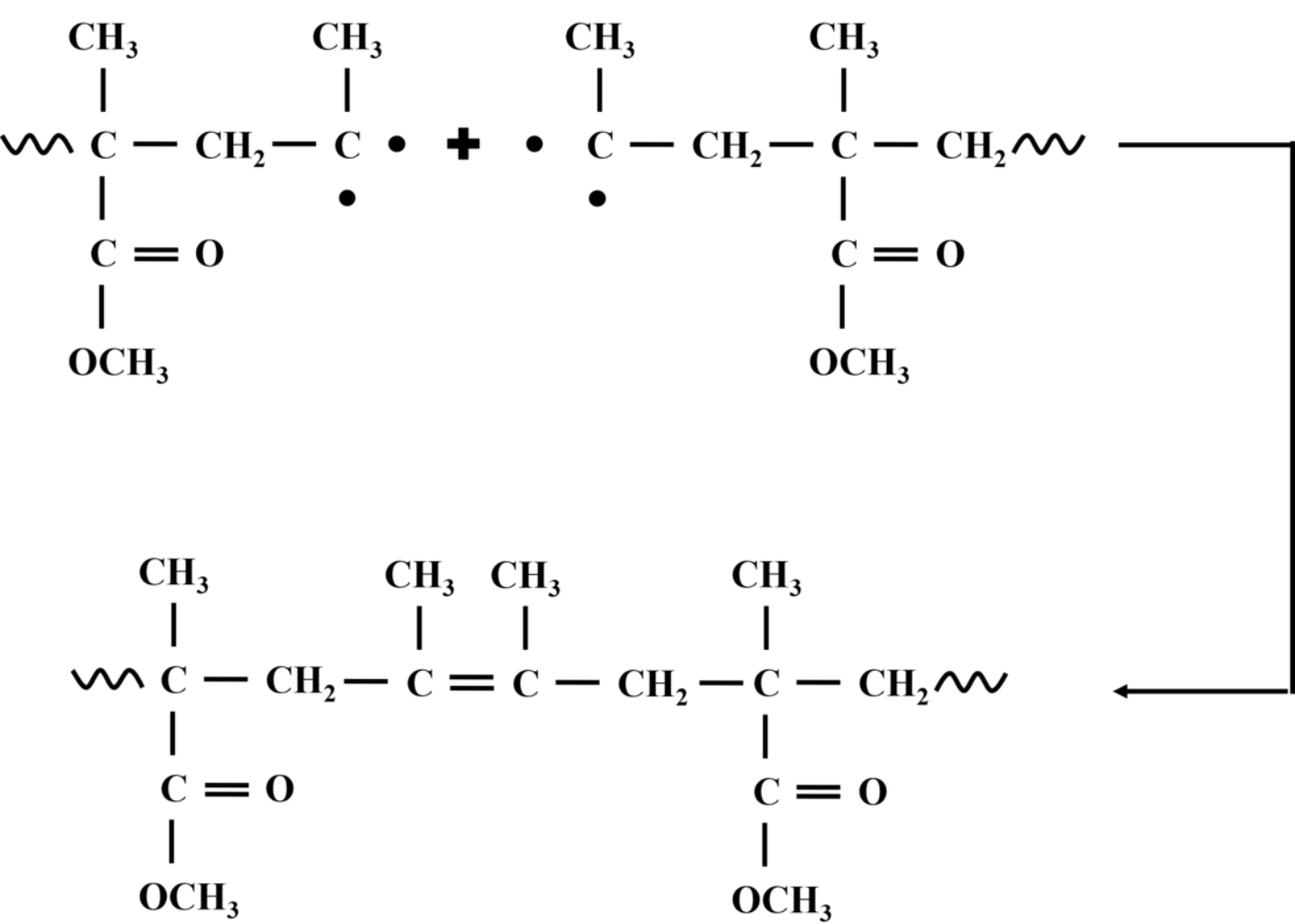

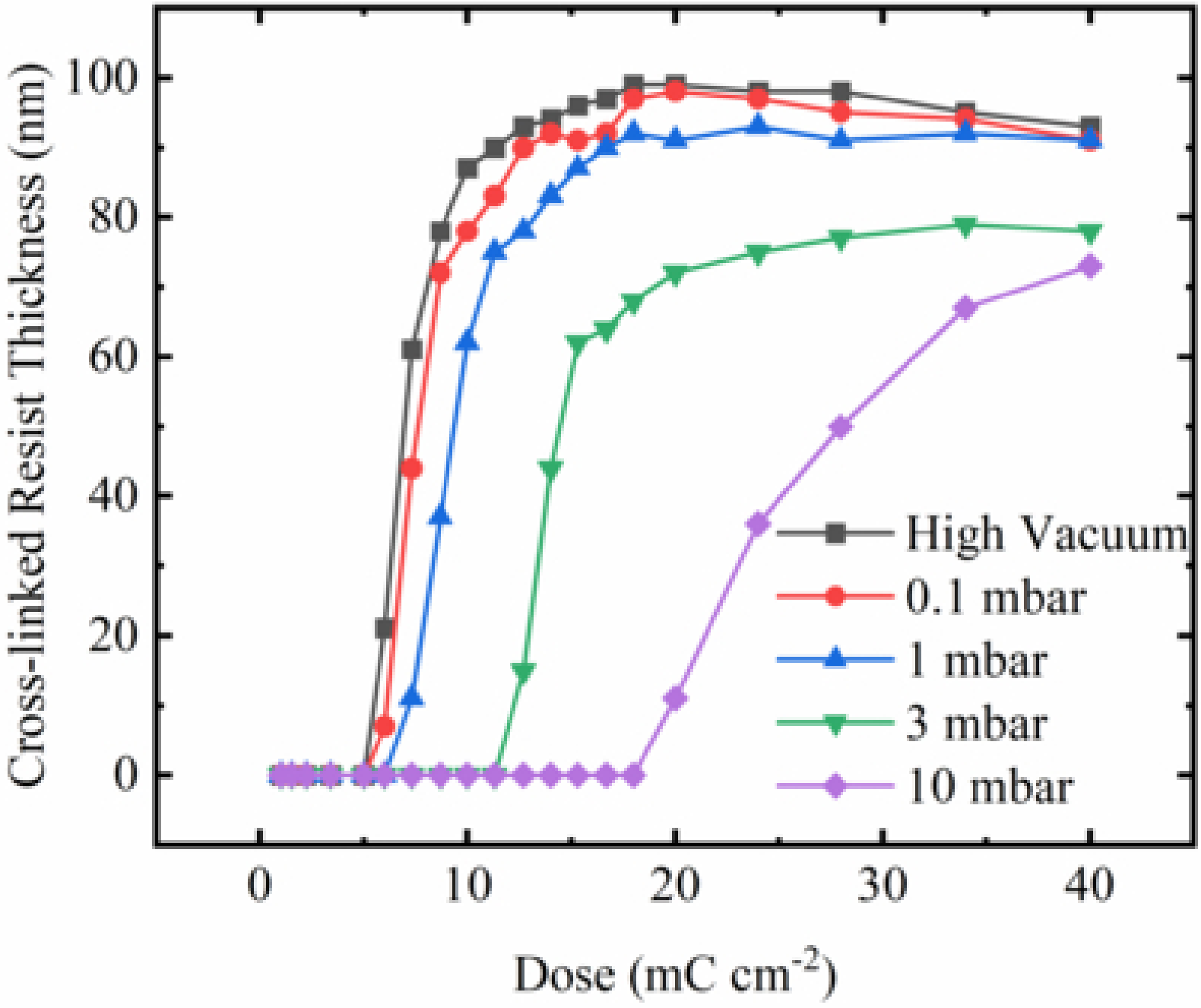
Cross-linked Resist Thickness (nm)
100
80
60
40
20
0
0
10
20
30
40
Dose (mC cm-2)
High Vacuum
0.1 mbar
1 mbar
3 mbar
10 mbar

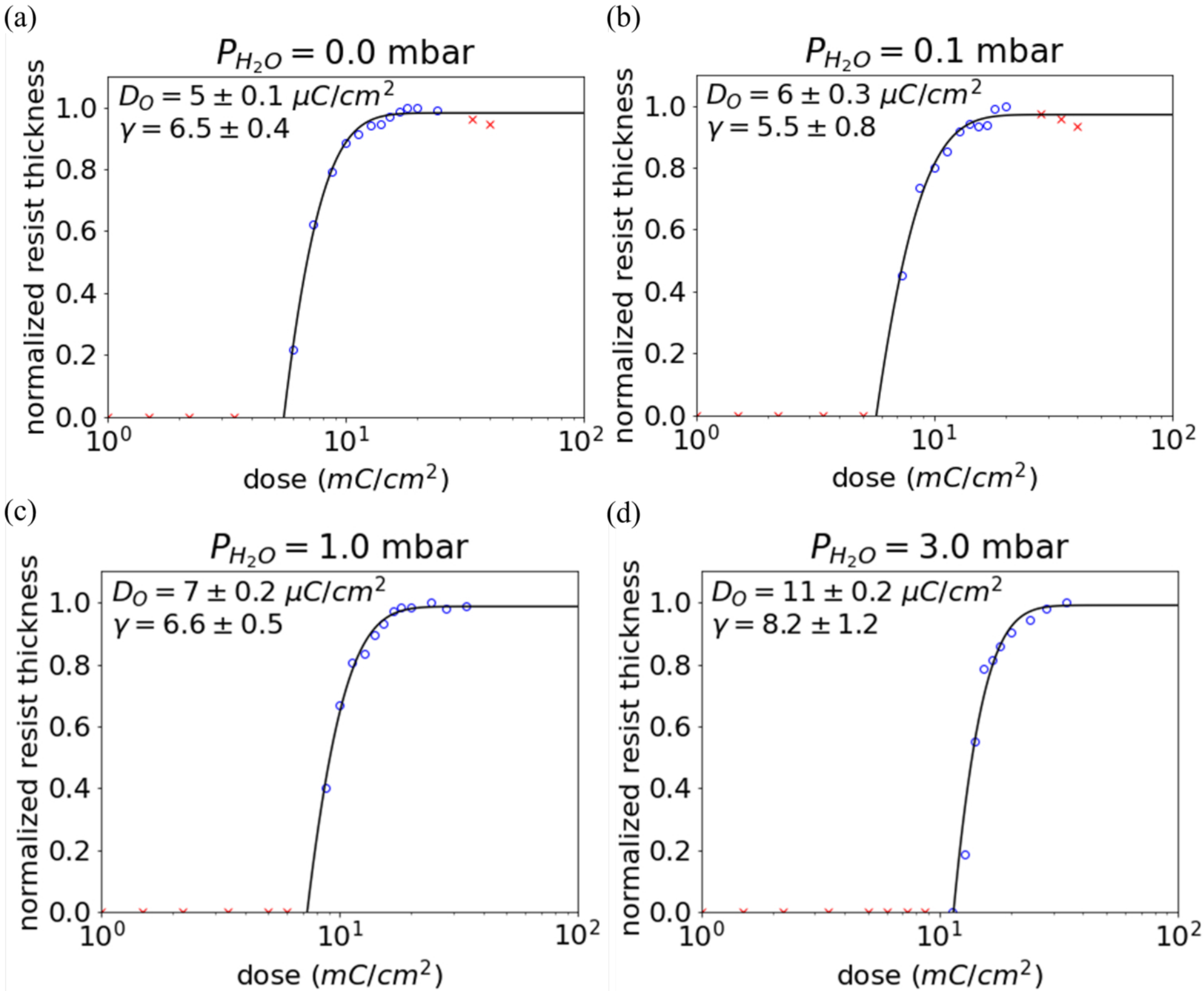
(a)
$P_{H_2O} = 0.0$ mbar
$D_O = 5 \pm 0.1\ \mu C/cm^2$
$\gamma = 6.5 \pm 0.4$
(b)
$P_{H_2O} = 0.1$ mbar
$D_O = 6 \pm 0.3\ \mu C/cm^2$
$\gamma = 5.5 \pm 0.8$
(c)
$P_{H_2O} = 1.0$ mbar
$D_O = 7 \pm 0.2\ \mu C/cm^2$
$\gamma = 6.6 \pm 0.5$
(d)
$P_{H_2O} = 3.0$ mbar
$D_O = 11 \pm 0.2\ \mu C/cm^2$
$\gamma = 8.2 \pm 1.2$
normalized resist thickness
dose (mC/cm^2)

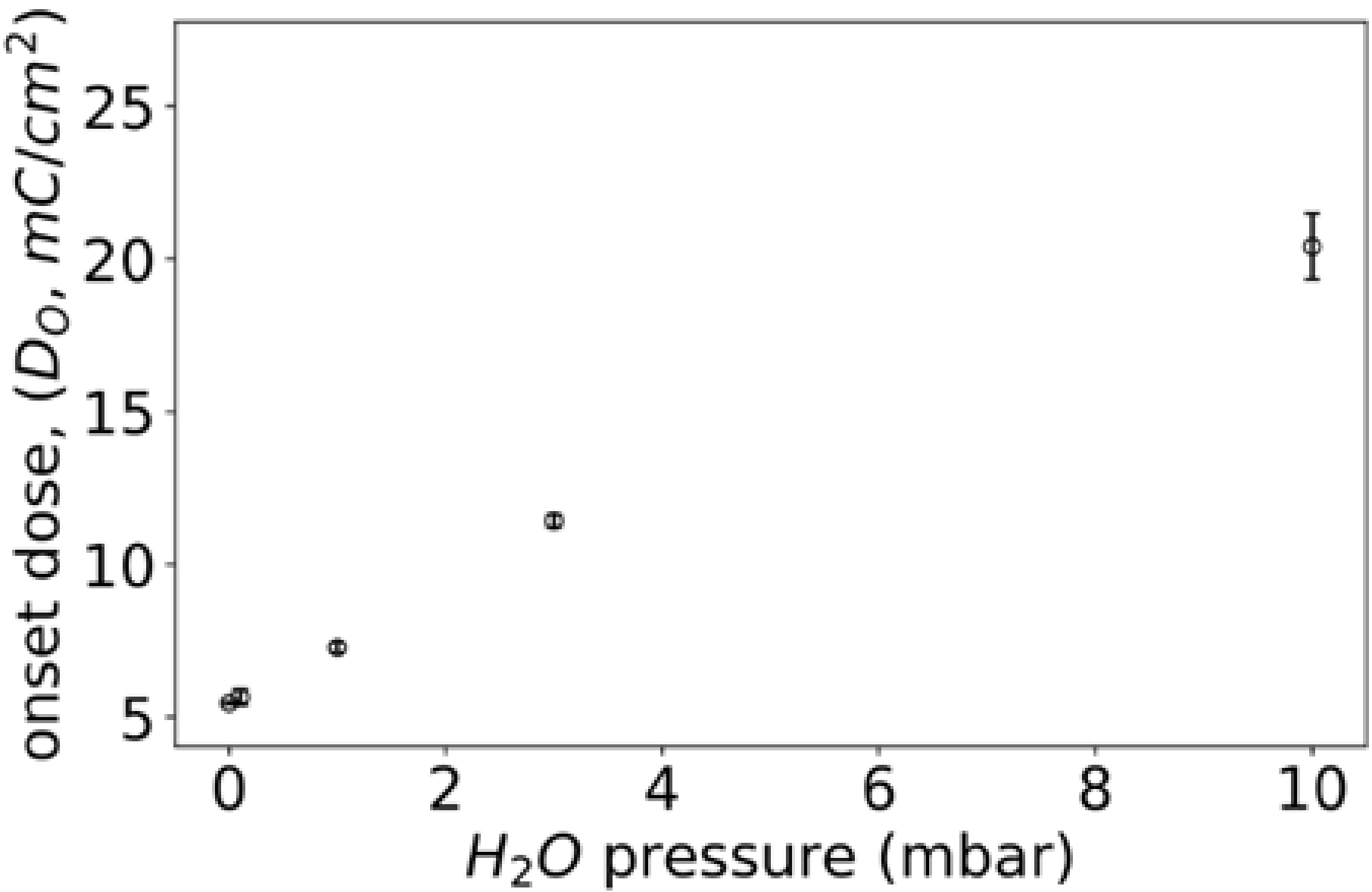
onset dose, (D_O, mC/cm^2)
5
10
15
20
25
0
2
4
6
8
10
H_2O pressure (mbar)

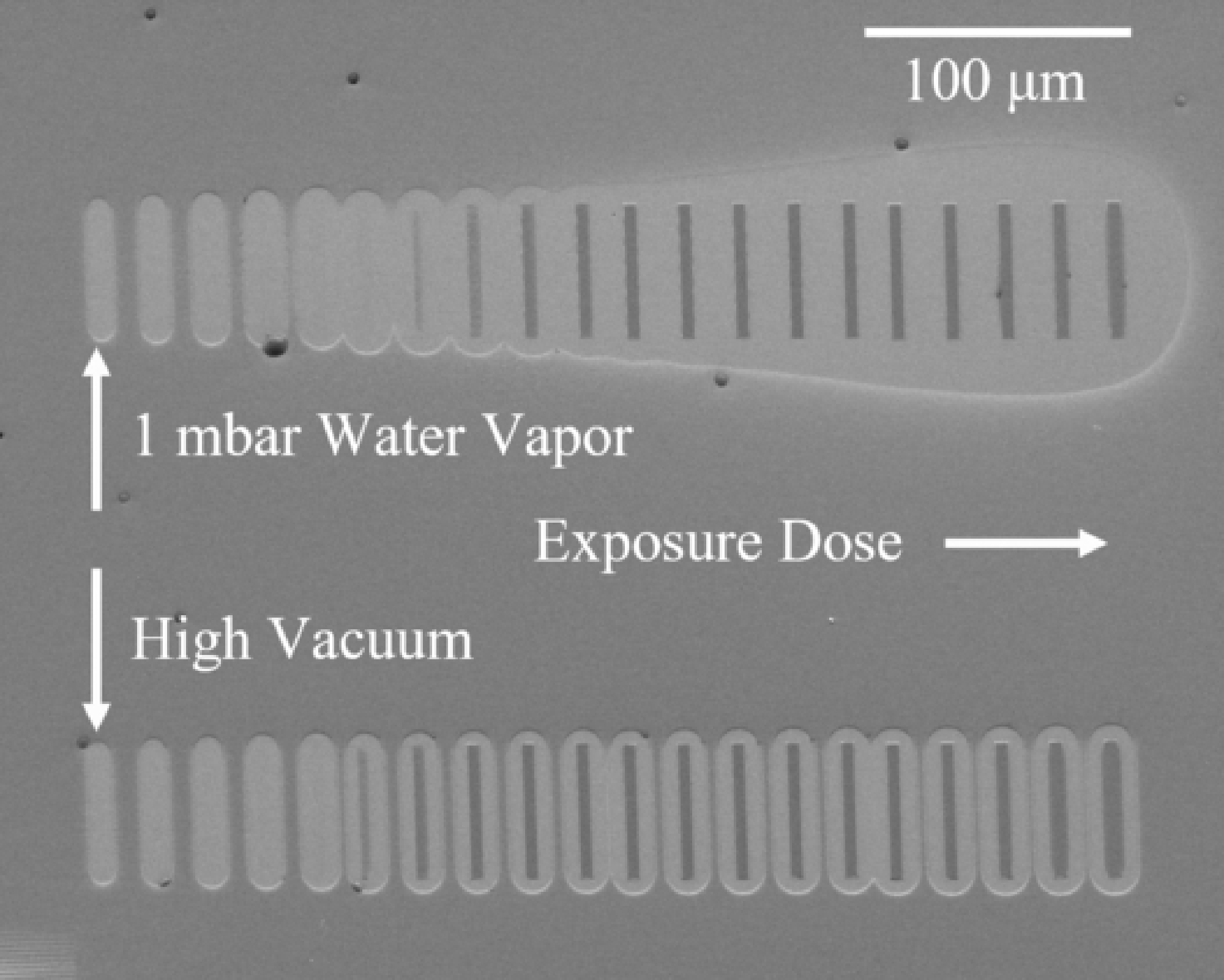
100 µm
1 mbar Water Vapor
Exposure Dose
High Vacuum

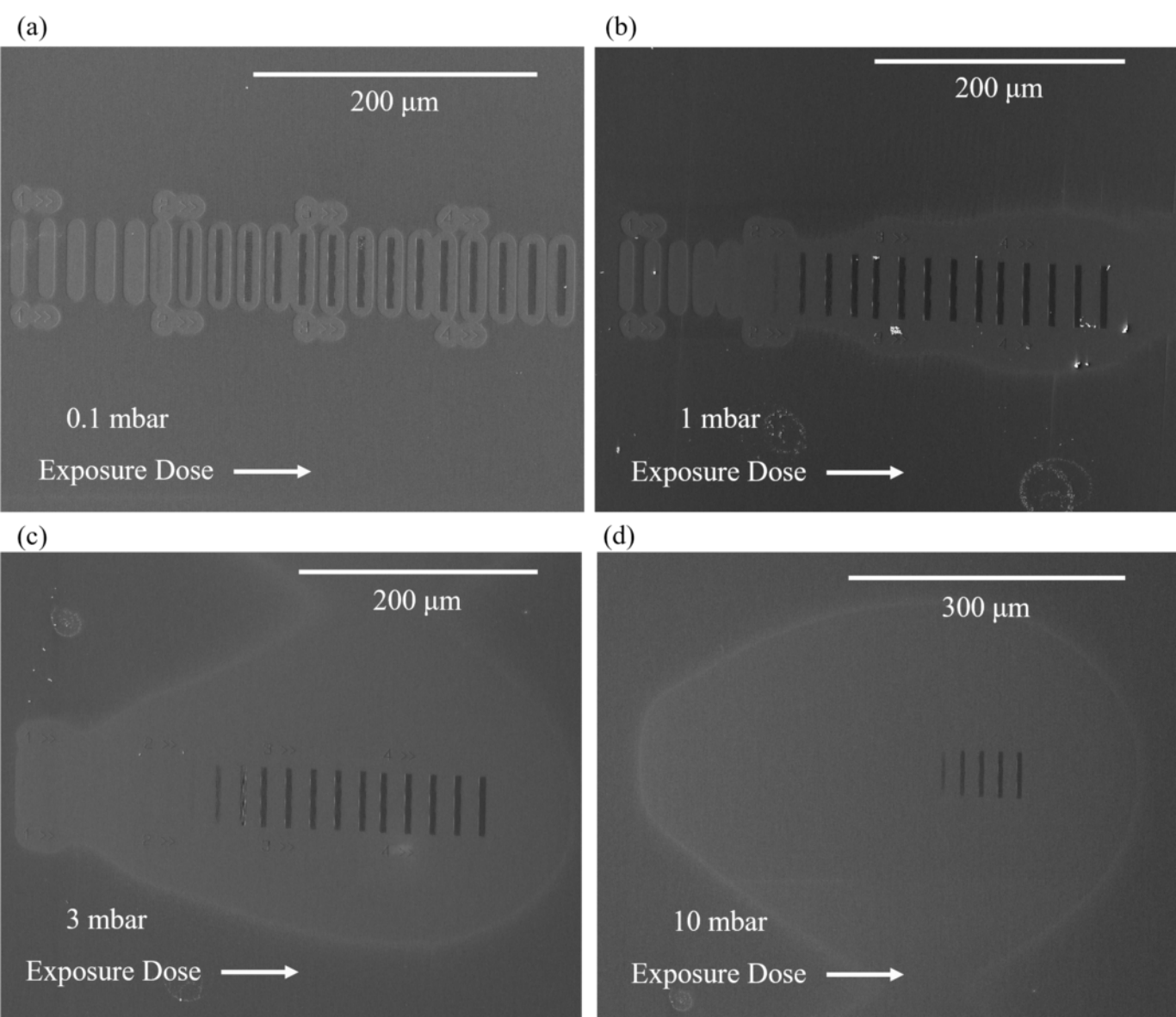
(a)
200 µm
0.1 mbar
Exposure Dose
(b)
200 µm
1 mbar
Exposure Dose
(c)
200 µm
3 mbar
Exposure Dose
(d)
300 µm
10 mbar
Exposure Dose

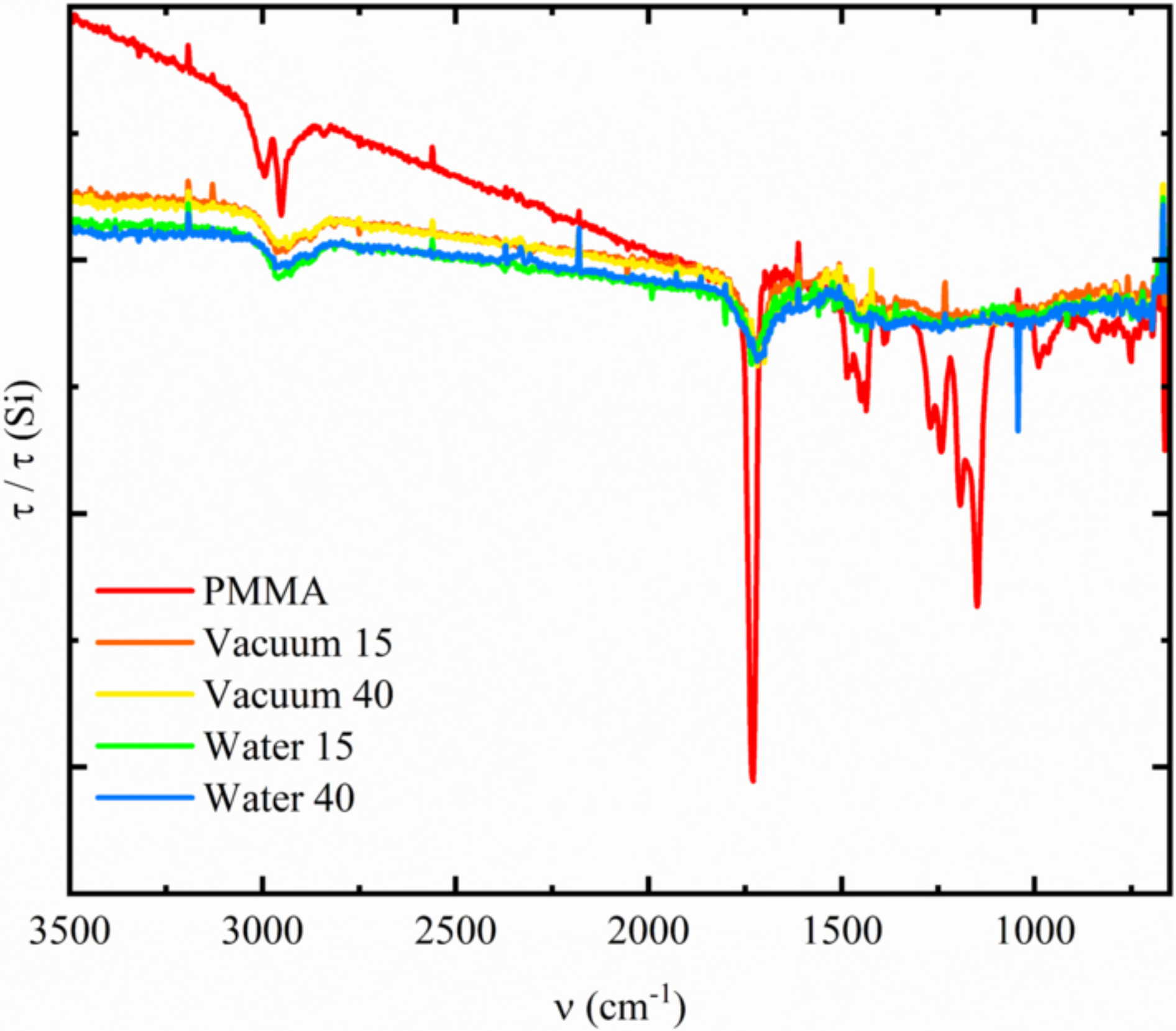
τ / τ (Si)
PMMA
Vacuum 15
Vacuum 40
Water 15
Water 40
3500
3000
2500
2000
1500
1000
ν (cm-1)

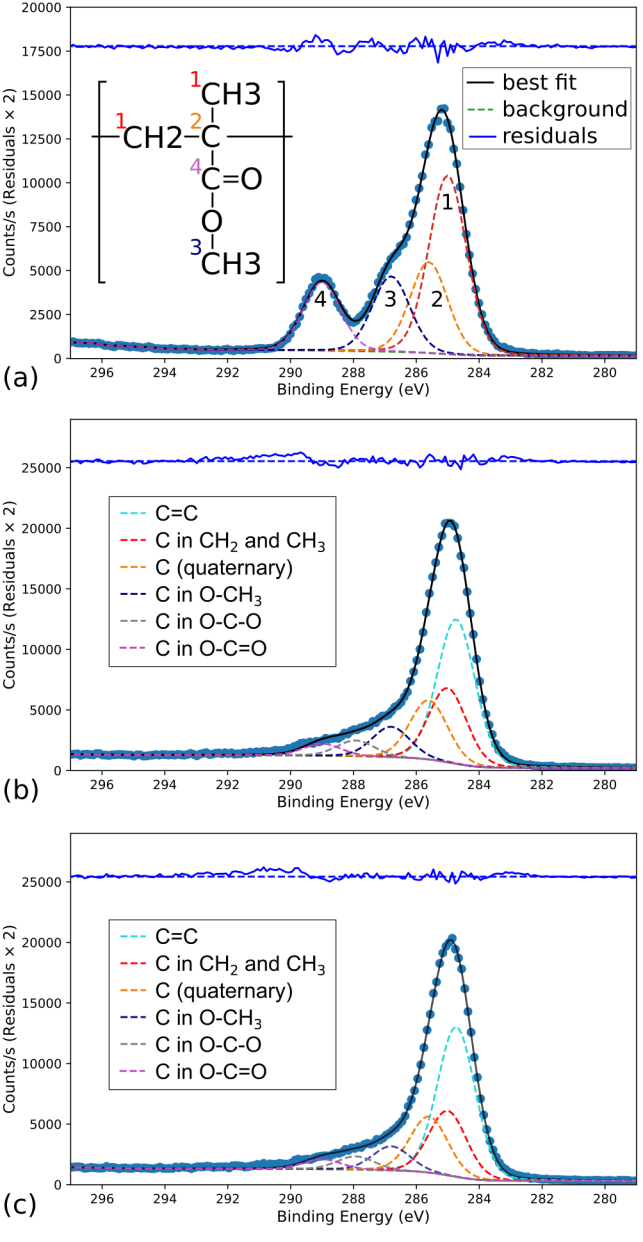
Counts/s (Residuals x 2)
Binding Energy (eV)
best fit
background
residuals
1
2
3
4
(a)
C=C
C in CH2 and CH3
C (quaternary)
C in O-CH3
C in O-C-O
C in O-C=O
(b)
(c)